Environmental Earth Sciences (2023) 82:146
https://doi.org/10.1007/s12665-023-10809-2

ORIGINAL ARTICLE

Moisture expansion of tuff stones and sandstones

Siegfried Siegesmund[1] · Christian J. Gross[1] · Reiner Dohrmann[2,3] · Bernd Marler[4] · Kristian Ufer[2] · Tobias Koch[1]

Received: 17 December 2022 / Accepted: 10 February 2023 / Published online: 10 March 2023

Abstract

Volcanic tuffs and sandstones have been used as natural building stones in the construction of monuments and buildings over the millennia of human history. Progressive weathering over time (e.g., temperature fluctuations, moisture uptake, variations in humidity, precipitation, the input of modern-day pollutants or salt crystallization) lead to damages in the internal structure of the stone. Scaling and layer-parallel flaking of rock fragments result from these types of damage-causing processes, especially when swellable clay minerals are present that lead to the generation of stresses in the rock fabric. Tuff and sandstone samples that exemplify these types of damages are investigated in this study, which were used in the construction of cultural heritage sites in Armenia, Mexico, Germany and Switzerland. Comparisons are made between these rock types considering that they show strong variations in fabric heterogeneity, grain sizes, mineralogical composition (e.g., swellable clay- and zeolite-bearing minerals), and visible macroscopic features such as depositional layering. Comprehensive investigations have been carried out that include detailed petrographic analyses, XRD analyses for the determination of the swellable and non-swellable clay fraction and minerals of the zeolite group, the cation exchange capacity (CEC), detailed SEM surveys for determining the type and localization of clays and zeolites in the rock fabric, as well as defining the petrophysical properties (e.g., porosity, capillary water uptake, water absorption, hydric expansion and mechanical properties). Moreover, this study explores the possible interaction between swellable clay minerals and zeolites (mordenite, heulandite/clinoptilolite) by conducting swelling experiments with salts and solvents and fluid-exchange experiments with and without the presence of zeolites. To explain the damages caused by the expansion in the tuffs and sandstones, two principle modes of moisture expansion are discussed when swellable clay minerals are present in the rock. These are dominantly inner or intracrystalline swelling, and secondarily, intercrystalline or osmotic swelling. When no swellable clay minerals are present, the study explains the damages in tuffs and sandstones as the result of disjoining pressure, where a high percentage of microporosity plays a pivotal role.

Keywords Moisture expansion · Volcanic tuffs and sandstones · Clay and zeolite mineralogy · Petrophysical properties · Modes of swelling

Introduction

Volcanic tuffs and sandstones, like all natural stones used on buildings, are subjected to physical, chemical and biological weathering processes. In addition to the exposure and climatic influences, the internal structure of the natural stone is also of decisive importance for the weathering intensity. Furthermore, the mineral composition and grain bonding, porous rocks containing porosities ranging from 5 to 50%, the size, distribution and structure of the pore space is especially of great importance with respect to the weathering processes taking place (e.g., Fitzner 1988; Fitzner and Snethlage 1982; Putnis et al. 1995; Kocher 2005; Putnis and Maute 2000; Siedel 2010; Ruedrich et al. 2011; Pötzl et al.

✉ Siegfried Siegesmund
ssieges@gwdg.de

[1] Geoscience Centre of the University Goettingen, Goettingen, Germany

[2] Federal Institute for Geosciences and Natural Resources (BGR), Hanover, Germany

[3] State Authority of Mining, Energy and Geology (LBEG), Hanover, Germany

[4] Fakultät für Geowissenschaften, Institut für Geologie, Mineralogie und Geophysik, Kristallographie, Ruhr-Universität Bochum, Bochum, Germany

2018a; Siegesmund and Snethlage 2014). Moisture transport and moisture balance in the rock is controlled via the connected pore space. The moisture content in the pore space and its distribution also affect the deposition and accumulation of contaminants. Crystallization processes of salt and ice in the pore space as well as hygrothermal strains caused by moisture and temperature changes are considered to be crucial damage factors.

Under the permanent influence of external factors such as moisture, temperature changes and pollutant input, zones of increased moisture and/or salt stress develop in the porous natural stone fabric, whereby the fabrics are subjected to particularly high stresses (Snethlage and Wendler 1997). Such zones are often linked to primary fabric heterogeneities in the natural stone, e.g., clay pebbles, clay mineral rich layers (Grassegger 1998; Ruedrich et al. 2011), bedding joints, and the alternation between porous matrix and dense, cemented fabric domains (Siedel 1998). In the buildup of stresses leading to mechanical destruction, moisture-related dilatation processes in particular play a decisive role in the porous fabric, as well as the additional effects of salts (Steiger et al. 2011). The evaluation of certain sub-processes for the destruction of natural stone fabrics is still controversial (see Nägele et al. 1992; Kocher 2005; Wangler and Scherer 2008, Pötzl et al. 2018a; Elert and Rodriguez-Navarro 2022).

Moisture expansion is a deformation phenomenon and is known in the literature as hygric (in the range of 0 and 95% relative humidity) and hydric (when in contact with water or immersed) expansion and contraction due to moisture exchange. In this study, the moisture expansion was investigated by immersing the samples in a tray of water, which demonstrates hydric expansion. Moreover, we also compared our results with the literature, where references are made to hygric expansion. The term hygric- and hydric expansion is not strongly differentiated in the literature. Both terms are interchangeably used. In most cases, hygric is used for moisture expansion.

Of great importance regarding the weathering of volcanic rocks and sandstones is the hygric swelling process (Kocher 2005; Snethlage et al. 1995; Benavente et al 2008, Sebastián et al. 2008). Especially in connection with temperature-induced stresses, the swelling and shrinking of rocks leads to a permanent stress in the rock fabric. Thus, scaling and layer-parallel flaking of rock fragments are attributed to these types of damage processes, which are evident in important cultural heritage sites, for example in Armenia, Mexico, Switzerland and Germany (Figs. 1, 2). Numerous authors thereby assume that the hygric strain can essentially be attributed to the hydration of the interlayer cations of very fine-grained (< 2 µm) layered and expandable 2:1 aluminosilicate (clay minerals), which are part of the mineralogical composition of the rock (De la Calle and Suquet

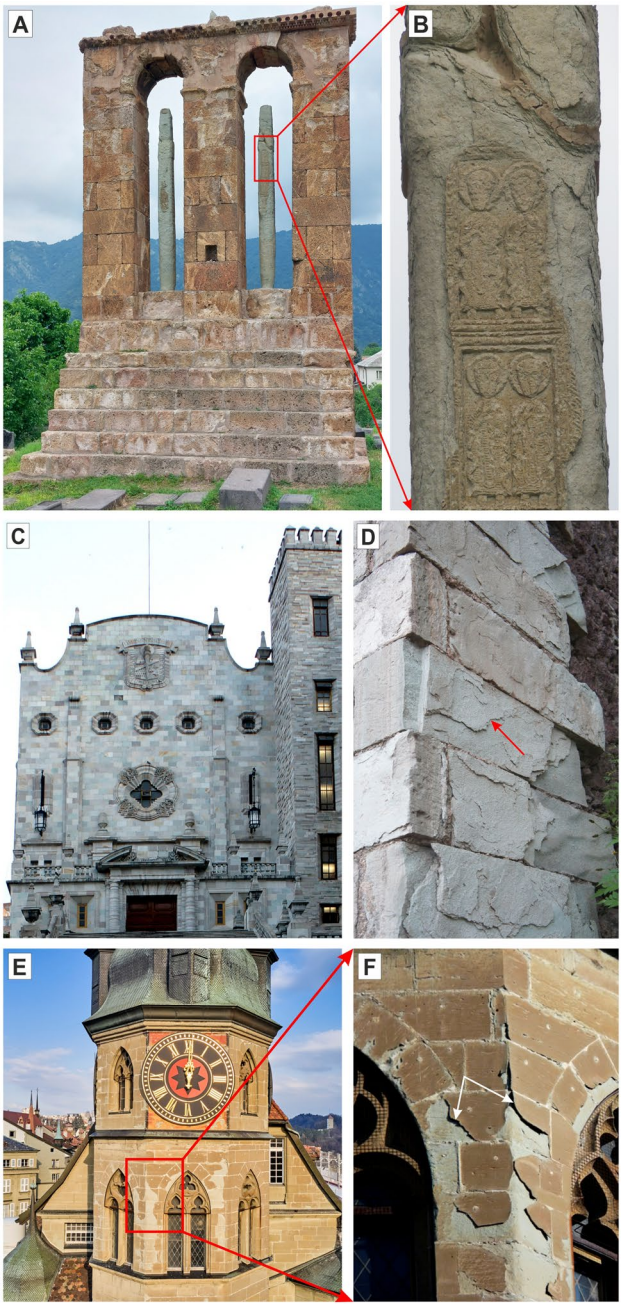

Fig. 1 Cultural heritage sites constructed using tuffs and sandstones and the types of damages caused by weathering. **A** Funerary monument with two inscribed stelae constructed using the very fine-grained tuff variety Blue Sevan at the Odzun Church (Lori Province, Armenia), **B** close-up of the right stelae showing extensive damages caused by layer-parallel flaking, **C** the laminated Loseros tuff used for the façade of the central building of the University of Guanajuato (Guanajuato, Mexico), **D** typical scaling feature of the Loseros tuff showing strong damages on the façade ashlars (red arrow), **E** present-day photo of the City Hall building erected with the Villarlod molasse sandstone in Fribourg, Switzerland. Many of the peeling sandstone scales have been removed. **F** Earlier photo showing a close-up of some of the peeling sandstone scales

Fig. 2 Exemplary damage features in some of the investigated tuffs and sandstones. **A** Columns constructed from Blanca Pachuca tuff showing layer-parallel peeling of the stone (white arrow), **B** extensive flaking damage of Cantera Verde used for doorway lintels similar to the Armenian Blue Sevan tuff, **C** massive damage (white arrow) to the Schleerieth sandstone which lacks swellable clay minerals, **D** close-up of scaling damage in the Loseros tuff, **E** example of the type scaling into rock fragments in the Mexican Cantera Rosa tuff, and **F** detail of the weathering damage in the Baumberger calcareous sandstone

1988; Dixon and Weed 1989; Moore and Reynolds Jr 1989; Graf v Reichenbach and Beyer 1995; Kocher 2005). Other authors attribute the essential importance to the formation of a hydrate shell around the minerals that are connected with the presence of micropores (Stockhausen 1981). The decisive factor for progressive damage is not only the hygric swelling dimension, but also the speed and relative movement of the associated solutions, which are controlled by the capillarity and the water vapor diffusion resistance of the materials.

Two principle modes of swelling are discussed when clay minerals are present in a natural building stone: (1) inner- or intracrystalline swelling which occurs in the interlayer region of expandable clay minerals and (2) intercrystalline or osmotic swelling which acts between clay particles. Movement of water by osmotic forces may cause non-equilibrium swelling processes in clay-rich media (Mitchell 1993). Redistribution of porewater is driven by thermodynamic equilibria based on chemico-osmotic and capillary forces (Bock et al. 2010). The selected rocks differ mainly in their pore space properties and the type, amount and location of the clay minerals they contain. These factors are of crucial importance, because the investigated hydric swelling processes are either caused by swelling clay minerals or a disjoining pressure, triggered by the interaction of surface forces with a high micropore fraction in the nanometer

range (Ruedrich et al. 2011). Pötzl et al. (2018a) could show that especially the Hilbersdorf tuff variety (HR), which has been shown to lack swelling clay minerals, has the strongest hydric strain. Consequently, swelling associated with the presence of expandable clay minerals can be excluded for the Hilbersdorf sample. When analyzing the pore radius distribution, it becomes evident that the variety HR has pores in the range of < 2 nm. This is the basis for the effect known as disjoining pressure originally defined by Derjaguin and Kusakov (1936). Therefore, micropores are of special importance because the disjoining pressure can only develop in these smaller pores.

An active proof of the primary swelling mechanism in the presence of swellable clay minerals in tuff rocks used as building stones, however, was provided by e.g. Pötzl et al. (2018a). By selectively exchanging the interlayer cations in the clay minerals and subsequently changing the swelling behavior of the rocks, it was demonstrated that the intracrystalline swelling mechanism is the predominant mechanism for swelling in the investigated tuffs that contain swellable clay minerals. Confirmation of the intracrystalline swelling process is achieved by selectively blocking the hydration of the clay mineral interlayers, and thereby suppressing their expansion. A second swelling experiment, in which fluid exchange served to verify intercrystalline or osmotic swelling, confirmed the almost insignificant contribution of osmotic swelling to the overall swelling process. These results were verified in the earlier work of Wangler and Scherer (2008).

Numerous damage phenomena observed in sandstones as well as volcanic tuffs used as building stones are attributed to the effect of salt loads (see examples in Fig. 2). Thus, surface-parallel scaling can be explained by salt accumulation and the resulting differences in hygric swelling behavior due to the formation of quasi-stationary moisture fronts (Wendler 1991; Ruedrich and Siegesmund 2006), by the reduction of pore spaces in the near-surface rock zone (later scales), and the blockage of fluid transport by gypsum precipitation (Siedel 1998), or by the impregnation with consolidation agents (Siedel 1994; Bosbach and Hochella 1996; Bosbach et al. 1996; Pina et al. 1998; Rodriquez-Navarro and Doehne 1999; Pötzl et al. 2022a).

Various volcanic tuffs and sandstones were selected for the following investigations (Figs. 1, 2, 3). Sandstones and tuffs can reach length changes of up to 25%. The phenomenon of hygric length change in almost all porous building materials is always discussed in connection with the clay mineral content in the natural stone materials. For the selection of the investigated rocks, care was taken to ensure that various clay minerals existed. Some of the volcanic tuffs (Blanca Pachuca and Cantera Verde from Mexico and Noyemberyan, Armenia) also contain minerals of the zeolite group (mordenite, heulandite, and clinoptilolite) that may possibly interact with clay minerals in terms of mechanical swelling. Various German sandstones, such as the Schleerieth, Sander, Baumberger and the molasse sandstone from Villarlod (Switzerland) complete our selected samples for investigation. All rocks were analyzed in great detail with respect to their mineralogical composition, with emphasis also on clay mineral analysis and zeolite determination. Scanning electron microscopy was used not only for mineralogical analysis but also for the characterization of the corresponding minerals in the rock fabric. The determination of the cation exchange capacity (CEC) was also of particular importance. It is generally assumed that a high CEC value indicates an increased amount of expandable clay minerals, and thus, an increased swelling capacity. Depending on the method of CEC determination, this correlation may be questionable if the rocks contain a significant amount of zeolites, which even have larger CEC values than expandable clay minerals (for details see the section on zeolites).

In addition, the petrophysical properties were determined on the sample set, which included density, porosity, pore radius distribution, water absorption, capillary water absorption, and rock strength properties such as the Young's modulus. Hygric strain was analyzed for all samples. All samples were also pre-treated with different salt solutions (NaCl, KCl, CsCl) and also tetramethylammonium (TMA) in order to identify the swelling mode, e.g. short-range, ordered intracrystalline swelling and long-range, continuous osmotic swelling (e.g., Wangler and Scherer 2008; Pötzl et al. 2018a). From preliminary experiments and theoretical assumptions based on the individual cation exchange behavior of zeolites, e.g. (Barrer and Klinowski 1972) and clay minerals (van Bemmelen 1888), it was expected that a complex cation exchange interaction between clay minerals and zeolites could possibly exist. Thus, artificially produced model samples of different clay and zeolite compositions were also included in the sample set. These model samples were also subjected to salt loading to better understand the swelling mode.

Petrography, clay mineral determination and petrophysical properties

Microscopic analyses were done on the selected rocks utilizing a Zeiss Axio Imager.A2M petrographic microscope with an attached Axiocam 305 color digital camera. Standard thin section 30 µm in thickness were used. Moreover, all the samples were analyzed by the scanning electron microscope (SEM) at the Federal Institute for Geosciences and Natural Resources (BGR) to characterize the type and location of clay minerals and zeolites. A Zeiss Sigma 300 VP FEG scanning electron microscope operating at 10 kV was used

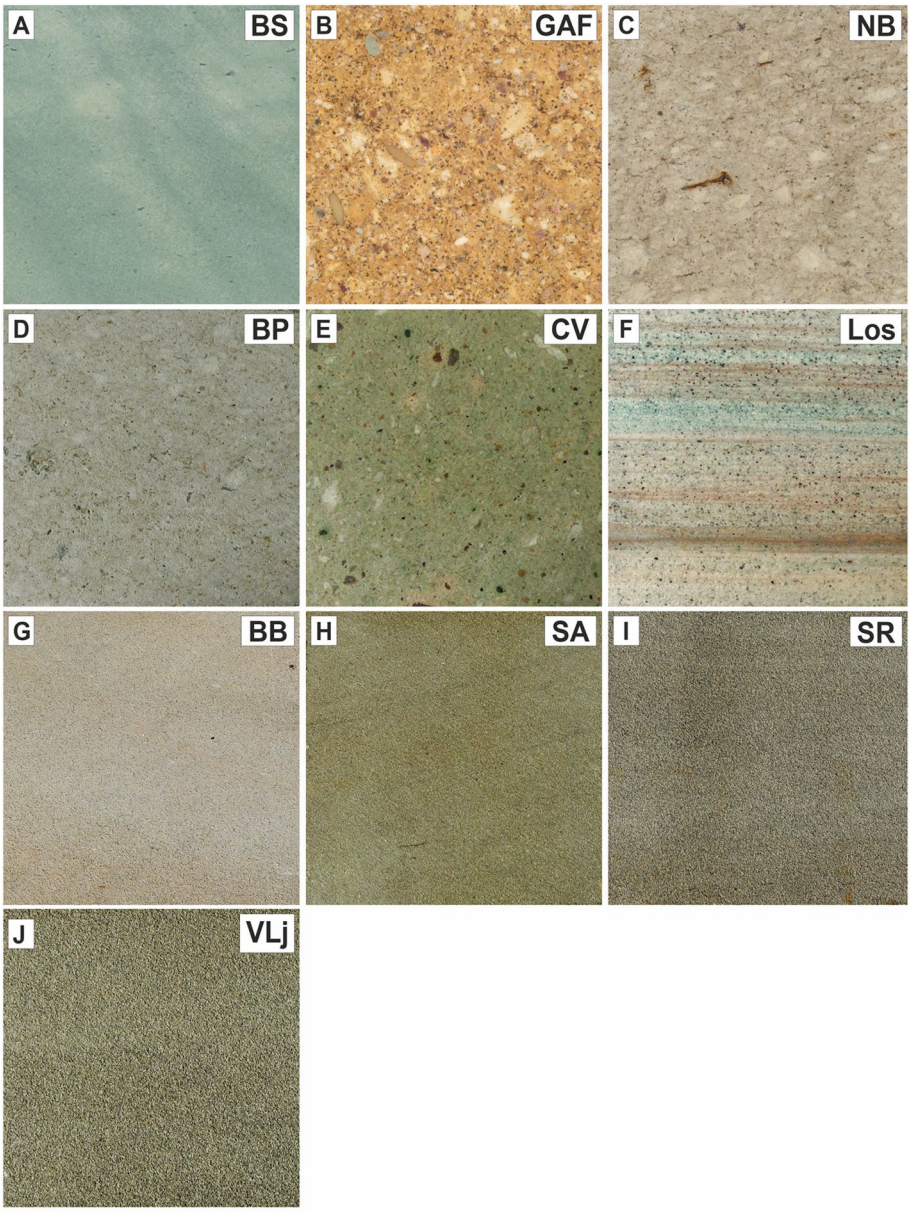

Fig. 3 Macroscopic fabrics of selected tuffs and sandstones. **A** Very fine-grained greenish Blue Sevan (also known as the Haghartsin Green, Armenia), **B** tuff variety known as the Golden Armenia Fine containing numerous volcanic lithoclasts, **C** white to grayish Noyemberyan tuff (Armenia) containing various volcanic lithoclasts, **D** light grayish Blanca Pachuca tuff from Mexico with numerous volcanic lithoclasts, **E** Cantera Verde tuff (Mexico), a somewhat mottled greenish stone containing different colored volcanic lithoclasts, **F** the finer grained, laminated volcaniclastic variety of the Loseros tuff (Mexico), **G** fine-grained, light yellowish gray calcareous Baumberger sandstone (Germany), **H** fine- to medium-grained, olive green sandstone known as Sander (Germany), **I** grayish to greenish medium-grained Schleerieth sandstone from Germany, and **J** medium-grained yellow greenish sandstone known as the variety Villarlod jaune (Switzerland)

to evaluate non-coated samples at the micro scale using the low vacuum mode.

For the mineralogical and geochemical characterization, X-ray diffraction (XRD) of whole rock samples and oriented slides of the clay fraction < 2 µm were used as well as X-ray fluorescence (XRF). Plausibility checks of the clay minerals by separation of clay fractions < 2 µm was performed for all but three samples with a very low CEC, where insignificant amounts of expandable clay minerals can be expected.

Oriented mounts were prepared to identify swelling clay minerals. A 1.5 ml sample suspension was deposited on circular (diameter = 2.4 cm) ceramic tiles. The suspension was filtered through the tile using a vacuum filter apparatus. After drying, XRD patterns of the oriented mounts were recorded. Furthermore, the specimens were stored overnight in an ethylene glycol (EG) atmosphere at 60 °C. The clay films are measured again after cooling to room temperature, representing EG conditions.

The three zeolite-rich tuffs were checked with the Rietveld refinement of the XRD powder pattern instead, using the disorder models of Ufer et al. (2012a, b). The so-called Rietveld method allows for the refinement of crystal-structure parameters (Rietveld 1969), and the refinement of individual scale factors for a phase mixture that can be used for quantification (e.g. Kleeberg et al. 2008) after careful plausibility checks. The Rietveld method is described by Monecke et al. (2001) as follows: "The method is based on a least-squares fit between step-scan data of a measured diffraction pattern and a simulated X-ray-diffraction pattern.

The simulated XRD pattern is calculated from a large number of parameters, including crystal-structure parameters of each component phase, a scale factor for each constituent phase to adjust the relative intensities of the reflections, parameters describing the peak profile and the background, and parameters simulating the instrumental aberrations as well as effects resulting from size-related strain, preferred orientation, and particle size.

A key feature of the quantitative analysis of phase proportions by the Rietveld method is that the phase abundances of the constituent phases can be directly calculated from the refined scale-factors." Quantification using the software Profex as a graphical user interface of BGMN (Doebelin and Kleeberg 2015) was performed for three zeolite-rich tuffs: Noyemberyan, Blanca Pachuca, and Cantera Verde. By XRD usually muscovite/illite were identified as micas, however, the presence of glauconite and biotite as observed by optical microscopy cannot be verified by XRD powder or from an oriented specimen of such mixtures.

The cation-exchange capacity (CEC) was determined after the copper(II) triethylenetetramine method of Dohrmann and Kaufhold (2009), modified from Meier and Kahr (1999). High CEC values indicate an increased amount of expandable clay minerals, and thus, an increased swelling capacity.

The moisture expansion of the samples was measured on cylindrical samples (diameter 15 mm and length 50 mm, respectively, 100 mm) under conditions of complete immersion in distilled water following the DIN 13009 (2000). The linear expansion was measured as a function of time by a displacement transducer with a resolution of 0.1 µm. Additional swelling experiments were performed with salts and solvents obtained from Fisher Scientific. Cationic pre-treatments were performed by soaking the sample in an approximately 3 M solution of chloride salt and subsequent washing in distilled water for several times.

To characterize the open (effective) porosity, hydrostatic weighing was performed on cubic samples (65 × 65 × 65 mm) after the DIN 772-4 (1998). To calculate the porosity, the water-saturated mass and the buoyancy mass of the vacuum water-saturated sample as well as the dry sample mass were used. Thus, directionally dependent measurements on the water uptake are done on the same sample (65 × 65 × 65 mm). Specimens were set with the bottom plane into 0.3 cm water and the weight increase over time was measured. The saturation degree (S-value) was determined by the quotient of unforced (atmospheric conditions) and forced (vacuum) water saturation (Hirschwald 1912).

Mercury intrusion porosimetry was used to acquire the pore radii distribution according to the DIN 66133 (1993). This was done by using the low (PASCAL 140) and high pressure (PASCAL 440) porosimeter units from Thermo Fisher Scientific. The water vapor diffusion resistance (µ value) was measured using the wet-cup method on samples with a diameter of 4 mm and a thickness of 10 mm (DIN EN ISO 12572 2017).

Results

Petrography and mineralogy

Blue Sevan (BS)

The Cretaceous Armenian tuff with the trade name Blue Sevan (BS) is characterized by a distinctive green color; although lighter zones appearing layer-like are also visible (Fig. 3A; see also Fig. 1B). These cut across a layering (discernible in thin section) and are defined by irregularly shaped dark green fragments disseminated throughout the stone. The fragments, which are altered to chlorite, range in size from the micrometer to the millimeter scale. Pötzl et al. (2018b) classified this tuff as a rhyolite using the system of Le Bas et al. (1986), a crystal tuff according to Schmidt (1981) and as an ash tuff by Fisher (1966).

The fabric is dominated by a cryptocrystalline matrix that comprises around 80% of the rock (Fig. 4A). Minor

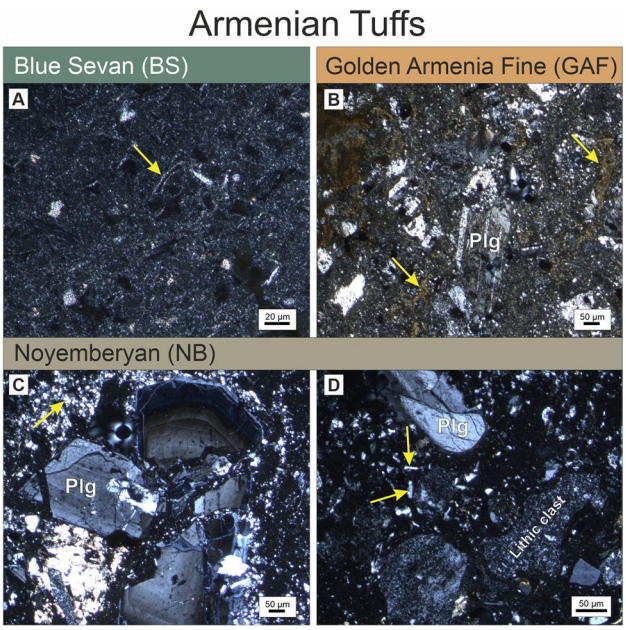

Fig. 4 Representative thin section fabrics of the Armenian tuffs. **A** Ash-rich matrix and opaque devitrified glass shards in Blue Sevan, **B** fabric in Golden Armenia Fine. Visible are deteriorated plagioclase phenocrysts embedded in an ash-rich matrix. Brownish zones may be corrensite, **C** large, zoned plagioclase phenocryst in Noyemberyan with fine-grained quartz in the ash matrix, and **D** fabric of the Noyemberyan tuff showing volcanic lithic clasts, plagioclase and small crystal feldspar laths embedded in an ash-rich matrix

amounts of quartz mono- and polycrystals occur as well as fine-grained K-feldspar phenocrysts embedded in the cryptocrystalline matrix. Trace amounts of weathered plagioclase is present showing polysynthetic twinning, which also show a coating with clay minerals under the SEM. Elongated phyllosilicate minerals are aligned parallel to the depositional ash layering. These show a greenish pleochroism and are interpreted to be chlorite. Idiomorphic apatite is present (identified by SEM and EDX) as well as muscovite. Relic glass shards appearing opaque in thin section are visible in the groundmass and show devitrification by the presence of extremely fine-grained crystals along the rims (yellow arrow in Fig. 4A). Minor amounts of analcime were detected by XRD (Table 1).

Throughout the entire fabric of the rock extremely fine-grained clay minerals (indicated by their higher birefringence in thin section) are aligned parallel to the layering in the cryptocrystalline matrix, which has also been confirmed by the SEM investigation. These are located at the grain contacts between the quartz and feldspar grains and are clay minerals with frayed edges. Moreover, thin sections were analyzed in the *X*, *Y* and *Z* plane, where in the *X*-plane round patches are visible that have a diameter of greater than 100 µm. These may represent possible spherules that have altered to clay minerals. XRD indicated that the clays consist of swellable interstratified smectitic (mixed layer) clay minerals, muscovite-illite, and minor kaolinite; CEC = 9 meq/100 g (Table 1).

Golden Armenia Fine (GAF)

The pyroclastic rock Golden Armenia Fine (GAF, Cretaceous in age) exhibits a light brownish yellow to yellowish-golden matrix. Embedded in this matrix is a wide range of volcanic lithic clasts that show reddish, white, light yellow, beige, light green, dark brown and black colors (Fig. 3B). These clasts range in size from < 1 mm to almost 1 cm. The shapes of clasts can be in some instances elongated with rounded edges to more angular fragments. A slight depositional layering can be discerned as indicated by oriented clasts. According to Pötzl et al. (2018b), the Golden Armenia Fine has the highest potassium contents and lesser sodium than the other tuffs in this study. Using the system of Le Bas et al. (1986), the GAF stone is a rock of rhyolitic composition, and in the system of Schmid (1981) a crystal tuff and lapilli tuff by Fisher (1966).

Compositionally, around 40% of Golden Armenia Fine (GAF) consists of a glass-rich matrix exhibiting high amounts of volcanic clasts and feldspar relics (Fig. 4B). Vitric fragments make up around 5%. K-feldspar phenocrysts are quite weathered, often showing alteration to sericite along the crystal edges. Deterioration of K-feldspar also takes the form of a pitted structure. Traces of plagioclase shows polysynthetic twinning. Opaque minerals occur in trace amounts and can be found as inclusions in K-feldspar. Somewhat rounded polycrystalline quartz clasts are also observable. Rare biotite can be observed in thin section, prismatic apatites are visible under the SEM, and traces of augite have been detected by XRD (Table 1).

Clay minerals are concentrated in the groundmass as evident by the devitrification visible in thin section (Fig. 4B) and observable under the SEM with frayed edges. XRD identified two types of clay minerals consisting of minor illite/muscovite and a major occurrence of the expandable clay mineral corrensite with CEC = 3 meq/100 g (Table 1). Corrensite is a regular 1:1 interstratification of trioctahedral chlorite with either trioctahedral 2:1 layers consisting of smectite or vermiculite. The layering in corrensite (named after Prof. Carl W. Correns formerly from the University of Göttingen) yields a super structure of a repeating chlorite-swelling layer upon a chlorite-swelling layer, etc.

Noyemberyan (NB)

Noyemberyan (NB) is a very light gray to whitish and slightly greenish Cretaceous tuff (Fig. 3C). Elongated white and gray lithic fragments define a weak lamination within a very fine grained ash-rich matrix. Some of the gray lithic fragments are rimmed by slightly orange to reddish margins and only few of these fragments can attain a size of approximately one centimeter. Based on Le Bas et al. (1986), Noyemberyan plots in the rhyolite compositional field. Using Schmid (1981) and Fisher (1966), this tuff can be classified as a crystal tuff or an ash-rich rock, respectively.

The fabric of this tuff consists of an ash-rich matrix making up 70% of the stone. Under polarized light the ash matrix is essentially opaque. Embedded in this fabric and making up around 30% of the tuff are numerous plagioclase and K-feldspar phenocrysts, and smaller, rounded quartz fragments. Some of the plagioclase phenocrysts show compositional zoning, polysynthetic twinning and are broken or fractured (Fig. 4C). Cryptocrystalline volcanic clasts are rounded or show irregular shapes (Fig. 4D). Calcite occurs associated with some highly broken feldspar crystals and minor muscovite can reach dimensions of 300 µm. Rare apatite and augite are also observable. Under the SEM large amounts of fibrous mordenite (confirmed by XRD), a mineral of the zeolite group, occurs as clusters along with clay minerals showing frayed edges. Intracrystalline swellable smectitic mixed layers (illite–smectite) were identified by XRD on separated clay fractions along with muscovite/illite; CEC = 9 meq /100 g

Table 1 Mineralogical composition determined by XRD in the tuffs and sandstones investigated, the cation exchange capacity (CEC) and the specific surface area (SSA) by N2 adsorption

Samples	CEC (meq/100 g)]	SSA (m^2/g)	Phyllosilicates						Zeolites		Other minerals determined by XRD							Optically determined													
			Inner-crystalline swellable minerals			Non-swellable minerals																									
			Smectite	Smectitic mixed layer	Corrensite	Muscovite/illite	Chlorite	Kaolinite	Mordenite	Heulandite/clinoptilolite	Analcime	Quartz	Cristobalite	K-feldspar	Plagioclase	Augite	Calcite	Glass shards/matrix	Apatite	Glauconite	Biotite	Tourmaline	Barite	Rutile	Zircon	Epidote	Opaques	Lithic fragments			
Blanca Pachuca (BP)	12	17	xx						x	xxx		xx	x	x	x			x			tr									
Cantera Verde (CV)	6	26	x			x	x	?	x	xx			xx	xx				x												
Noyemberyan (NB)	9	3		x		x			xxx			x		x		x	x		r				tr							
Loseros (Los)	5	12	x	xxx				x				x		xx	x		x				tr						tr			
Blue Sevan (BS)	9	8		xx		x		x			x			x				x	tr											
Villarlod (VLj)	4	5.3	xx			x	x					xxx		xx	xxx		xxx			x						tr				
Baumberger (BB)	4	11.9	xx			x						xx					xxx		tr	x	tr									
Golden Armenia Fine (GAF)	3	6			xx	x						x		x		x		x			r						tr			
Sander (SA)	3	5.1		x		x	x	x				xxx		xx	xx				tr			tr		tr				tr		
Schleerieth (SR)	2	4.5				x	xx					xxx		xx	xx		x		tr			tr			tr		tr		x	

Minerals determined by optical means are also listed. The semiquantitative occurrence for the XRD are represented by x's and indicate: xxx = dominate phase, xx = major component, x = minor component, and ? = possible trace component. Optically determined: tr = trace and r = rare. Glass component in the Blue Sevan tuff was also detected by XRD

(Table 1). In contrast to the other Armenian or Mexican tuffs, barite was also detected by SEM and EDX.

Blanca Pachuca (BP)

The Pliocene tuff, known as Blanca Pachuca, is a light grayish rock containing dark gray lithic fragments and some reddish and black vesicular cinder clasts (Fig. 3D; see also Fig. 2A). Weathered pumice occurs as flattened, subrounded and angular clasts. Their size ranges from a few mm to > 1 cm. All these clasts are matrix supported in a very fine-grained ash-rich groundmass. Blanca Pachuca can be classified as a rhyolitic tuff (Le Bas et al. 1986) and as a crystal-rich ash using Schmidt (1981) and Fisher (1966).

Quartz is a major phase with minor twinned plagioclase and K-feldspar, which occurs as anhedral to subhedral crystals embedded in a cryptocrystalline ash matrix (Fig. 5A). Some of the quartz crystals also show numerous inclusions. Traces of biotite are also present. Zeolite minerals, consisting of considerable amounts of heulandite/clinoptilolite, and clusters of needle-like mordenite along with swellable clay minerals (smectite) were identified by XRD; CEC = 12 meq/100 g (Table 1). These represent the alteration of the former glassy matrix, which shows extensive devitrification.

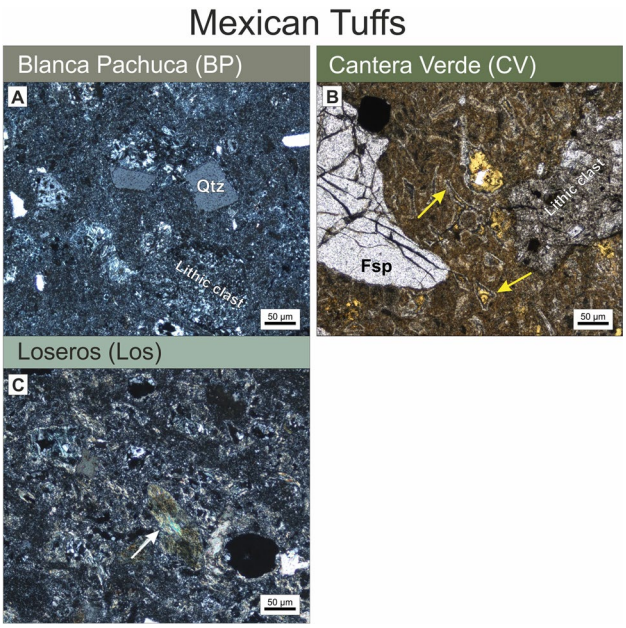

Fig. 5 Characteristic thin section fabrics and microstructures of the selected Mexican tuffs. **A** Cryptocrystalline matrix in the Blanca Pachuca tuff with quartz phenocrysts, weathered feldspar crystals and rounded lithic clasts, **B** well-preserved relic glass shards under transmitted light showing devitrification on the rims in the Cantera Verde tuff. Broken feldspar and lithic fragment also observable, and **C** the Loseros tuff exhibiting the ash-rich fabric. Also visible is an altered biotite

Cantera Verde (CV)

Macroscopically, the massive tuff Cantera Verde (Miocene in age) exhibits various shades of green from light to dark. This gives the stone a slightly mottled appearance. Considerable volcanic clasts ranging in size from less than a few mm to > 1 cm are embedded in a fine-grained ash-rich matrix (Fig. 3E; see also Fig. 2B). These consist of dark lithic fragments and altered and flattened pumice clasts showing a greenish coloration. White clay lenses occur that disperse in contact with water. The TAS system of Le Bas et al. (1986) places this stone in the compositional field of rhyolites. It can also be classified as a vitric ash tuff or a lapilli tuff using the systems of Schmid (1981) and Fisher (1966), respectively.

The overall fabric of Cantera Verde can be defined as an ash-rich hypocrystalline tuff (Fig. 5B). Crystals are strongly weathered and the glassy matrix strongly altered to zeolites and clay minerals. Approximately 7% of the crystals are matrix supported. The strong vitric component in this ash-rich stone makes it essentially opaque under polarized light. Under transmitted light the glass shards are easily observable. Individual shards are rimmed by extremely fine-grained crystals that represent the devitrification process (yellow arrows in Fig. 5B). The dominant mineral constituents as determined by XRD are cristobalite, K-feldspar, and the zeolite mineral heulandite. K-feldspars are subhedral to euhedral and are in part fractured without no discernible orientation. Mordenite, heulandite, smectite, muscovite/illite and chlorite have been detected by XRD; CEC = 6 meq/100 g (Table 1). In thin section, a 0.1 mm altered muscovite flake was observed. The lithic fragments are almost opaque in polarized light, with the exception of very fine-grained twinned plagioclase inclusions.

Loseros tuff (Los)

The Loseros tuff (Oligocene in age) is a well-sorted and fine-grained volcanoclastic rock. The characteristic feature of this stone is its distinctive laminated structure (Fig. 3F; see also Fig. 2D). These laminations show different thicknesses, displaying colors ranging from different shades of green, reddish brown, and lighter gray zones, sometimes purple and whitish. Distinct thin layers or bands are also visible showing greenish and reddish-brown laminations. Disseminated throughout the rock are numerous dark detrital clasts (black to reddish-brown) and millimeter-sized phenocrysts. These are embedded in a fine-grained ash-rich matrix containing abundant calcite. López-Doncel et al. (2013) identified two

distinct types, a fine-grained and a coarse-grained variety. Compositionally, the Loseros tuff plots in the dacite field of the TAS diagram. Utilizing the system of Schmid (1981) and Fisher (1966), this stone classifies as a lithic tuff or as an ash tuff, respectively.

Under transmitted and polarized light, the laminations are clearly visible, which are associated with the reddish-brown layers. These are essentially opaque zones of the ash-rich matrix. Quartz, K-feldspar, plagioclase, calcite and lithic fragments are the main mineral constituents. Both feldspars are angular to subhedral, whereas quartz only occurs as angular crystals. Trace amounts of biotite occur exhibiting considerable alteration. Opaques comprise around 10% of the stone. In thin section, the groundmass is made up of extremely fine-grained crystals representing the devitrification of the glassy components in the ash matrix. A low amount of relic glass shards remains, and the fabric can be defined as hypocrystalline to holohyaline (Fig. 5C). Individual grains are cemented with a calcitic and clay matrix. The SEM and XRD investigation (Table 1) has revealed considerable swellable clay minerals (smectite plus interstratified illite–smectite) and minor kaolinite; CEC = 5 meq/100 g.

Baumberger sandstone (BB)

The upper Cretaceous (Campanian) Baumberger calcareous sandstone is a fossil-rich, fine-grained, yellowish gray to creamy-colored sedimentary rock (Fig. 3G; see also Fig. 2F). Rust colored streaks are probably due to the weathering of the mineral glauconite, which leads to the formation of the iron hydroxide mineral goethite. Moreover, surface oxidation of glauconite may contribute to the yellowish stone coloration. Macroscopically, glauconite is evenly distributed throughout the stone as evidenced by the dark, fine-grained minerals (Fig. 3G). No macroscopic layering is visible in hand specimen.

The most dominant framework mineral is calcite and makes up around 70% of the stone. This is differentiated into carbonate clasts, micritic calcite cement, fossil fragments and coarser calcite, probably due to solution-precipitation processes. The overall fabric of the Baumberger sandstone is shown in Fig. 6A. Quartz appears as angular detrital grains that show little rounding and ranges in size from around 50–300 µm. It comprises around 16% of the stone. Glauconite shows both green to brown colors in transmitted light, suggesting a degree of alteration. In this particular sample, glauconite has been estimated to make up around 5%, although lower to higher amounts have been reported (Grimm 2018; Siegesmund et al. 2010). Minor detrital rock fragments occur consisting of feldspar, polycrystalline quartz and quartzite. The types of fossils that make up the carbonate component of the stone consists of fragments of foraminifera, echinoderms, ostracodes,

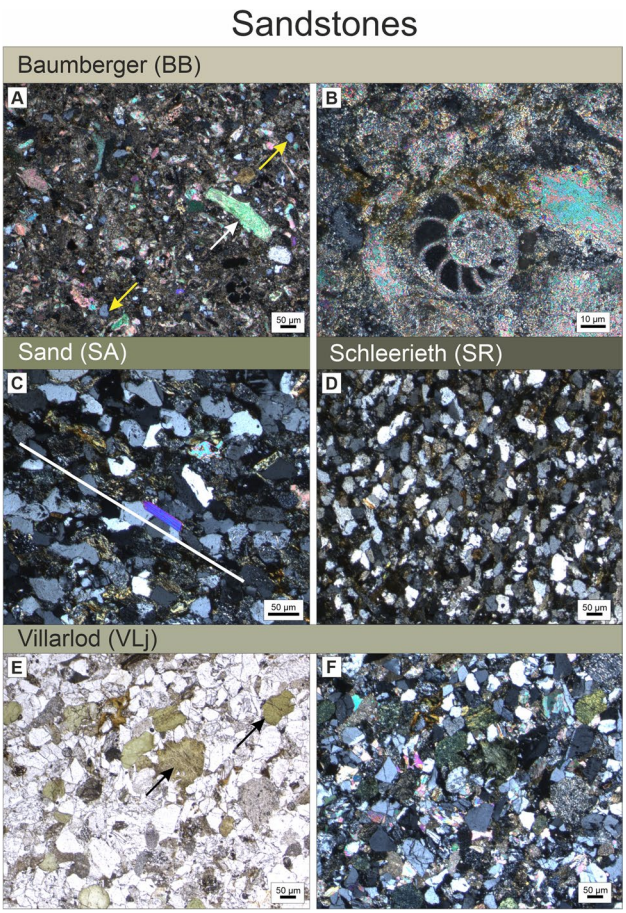

Fig. 6 Thin section fabrics of the selected sandstones. **A** Calcareous Baumberger sandstone—overall fabric consisting of fragmented fossils, micritic carbonate, coarser calcite grains and a muscovite flake, **B** well-preserved foraminifera fossil in the Baumberger sandstone, **C** the Sander fabric showing a sedimentary layering consisting of elongated quartz, phyllosilicates, altered feldspars and lithic fragments, **D** fabric of the Schleerieth sandstone, **E** transmitted light image of Villarlod jaune sandstone. Glauconite crystals are easily visible, and **F** same image under polarized light with abundant quartz, feldspar, calcite, fine-grained calcite cement and glauconite

bryozoans and fish scales (Grimm 2018). An example of a well-preserved foraminifera fossil is shown in Fig. 6B. By XRD the major clay mineral was identified as smectite with minor amounts of muscovite/illite, kaolinite was not identified; CEC = 4 meq/100 g (Table 1). Traces of large muscovite flakes have also been observed in thin section (Fig. 6A).

Given the high percentage of carbonate material, the rock can be classified as a calcareous sandstone of low maturity. Pore spaces of 0.2 mm in diameter or less, but mostly averaging 0.06 mm have been reported (Siegesmund et al. 2010). Because of the high carbonate composition, the weathering resistance is moderate to poor, which

results in dissolution features, breakouts of particle components, exfoliation and gypsum efflorescence (Fig. 2F).

Sander (SA)

Sander is an olive green, fine- to medium- grained sandstone with an age of Triassic Middle Keuper (Fig. 3H). Hematite coats many grains giving the stone a slightly faint rust coloration. It is a moderately to poorly sorted sandstone of low maturity and classified as a feldspathic litharenite (McBride 1963). Fabric analyses by Ruedrich et al. (2011) have shown that Sander has a relatively weak anisotropy, a median grain size of 0.098 mm and a sphericity in the *XZ*-plane of 0.859.

An overview of the grain supported fabric in thin section is shown in Fig. 6C, where a discernible sedimentary layering and grain orientation is visible as defined by the phyllosilicate minerals and elongated quartz grains. The main framework grain is quartz, which makes up around 60% of the rock. Not all quartz grains are elongated, but also subangular and slightly subrounded grains occur. Grain contacts are mostly located at points or elongated (Ruedrich et al. (2011). Some quartz grains are broken and show undulatory extinction. The SEM investigation also revealed an intensive intergrowth between chlorite and quartz. Feldspars consist of plagioclase and K-feldspar, showing alteration by secondary sericite. Twenty percent of the rock consists of lithic fragments identified as squeezed claystone by Demarco et al. (2007), but also traces of metamorphic rock fragments, shale and polycrystalline quartz. Phyllosilicates in decreasing amounts consist of chlorite (Fe-rich as determined by EDX), altered biotite and minor muscovite. Accessory minerals consist of apatite, rutile, tourmaline and opaques. The intergranular binding material comprises siliceous cement (quartz), minor feldspar, and combined clay-chlorite as an indirect cementing agent. Rarely calcite is observable.

XRD analyses as reported by Stück et al. (2013) indicated a large chlorite and illite content, swellable interstratified (illite–smectite) clay minerals and minor kaolinite; CEC = 3 meq/100 g (Table 1). SEM shows illite as long needle-like laths.

Schleerieth (SR)

Schleerieth is a light grayish green, medium-grained, moderately well-sorted sandstone with an age of Triassic-Lower Keuper (Fig. 3l; see also Fig. 2C). The grain size can be defined as coarse silt to fine sand and is classified as a litharenite of low maturity. According to Ruedrich et al. (2011), this sandstone has a strong anisotropy, a median grain size of 0.094 mm, and a sphericity of 0.833 in the *XZ* plane.

The Schleerieth sandstone fabric is grain supported, where the dominant mineral is quartz (around 80%) showing a subangular to subrounded grain shape (Fig. 6D). The grain contacts are located at points, but also elongated contacts are observable. Lithic fragments consist of volcanic and sedimentary rocks and amount to around 15% of the rock. Alteration of volcanic rock fragments is evident by their chloritization. Feldspars are strongly sericitized and make up about 3% of the stone. Muscovite, chlorite, tourmaline, apatite, zircon and opaque minerals are the main accessories. The binding cement occurs as periodic patches of calcite, syntaxial quartz and pseudo matrix. Clay aggregates produce a pseudo matrix and may be associated with altered clasts. These are found packed between quartz grains and results from the compaction processes (Demarco et al. 2008).

The XRD investigation indicated illite and traces of kaolinite, whereas swellable clay minerals are absent; CEC = 2 meq/100 g (Table 1). Under the SEM Fe-rich chlorite (chamosite) was detected and identified by EDX. These fill pore spaces and also occur as star-like spherical structures growing in open pore spaces.

Villarlod (VLj)

The Molasse de Villarlod is a fine- to medium-grained Miocene sandstone that occurs in three different varieties. These are the blue molasse, molassic sandstone and the yellow molasse. In this study, the Villarlod jaune (VLj; yellow molasse) was selected for comparison with the other sandstones in this investigation. Villarlod jaune is a brownish yellow to greenish stone with a visible porosity (Fig. 3J; see also Fig. 1F).

In thin section, the main phase is angular to subangular quartz, which makes up around 50–60% of the stone (Fig. 6E, F). Some quartz grains show sutured grain boundaries and extremely fine inclusions. Quartz can also be found in a polycrystalline form. Feldspars show alteration as indicated by the presence of sericite and comprise around 10–15% of the rock. K-feldspar is more abundant than plagioclase, which is also twinned. Calcite occurs in the grain fabric as individual twinned grains and as very fine-grained lime cement comprising 20–30% of the stone. The phyllosilicate, which contributes to the greenish and yellowish coloration is the mineral glauconite. It forms abundant individual grains in the fabric (as visible in transmitted light, Fig. 6E) and has similar grain sizes as the detrital silicate minerals. Chlorite occurs as a minor detrital component as well as traces of biotite and epidote.

The XRD analysis of the clay fraction identified smectite, and lessor amounts of muscovite/illite and chlorite; CEC = 4 meq/100 g (Table 1).

Petrophysical properties

Determining the petrophysical properties of natural stones is a prerequisite in assessing the quality of a building stone. Given the great diversity of volcanic rocks and sandstones with respect to their heterogeneity, origin, composition, fabric etc., 10 samples were collected to investigate their petrophysical properties. The data compiled in this study are listed in Table 2. The investigated rocks are mainly characterized as middle to highly porous, with porosities ranging from 14.9 to 29.5 vol%. The respective bulk densities range from 1.54 to 2.50 g/cm^3.

The pore size distribution of the Blanca Pachuca, Noyemberyan, Villarlod and Baumberger show a unimodal pore radii distribution (see Figs. 7, 8, 9). All other samples are characterized by a second maximum and can be described as bimodal. The values vary between 0.08 and 0.18 µm. The variation of the calculated mean pore radii distribution does not show a larger difference, which is in accordance with the observed lower variation in the porosity values. Micropores and capillary pores were evaluated in greater detail. BP, CV, Los and BS exhibit more than 79% of micropores. GAF, SA and SR have less than 50% micropores, while the remaining samples show consequently higher values of capillary pores (Table 2).

The capillary water absorption coefficient [kg/m^2*$\sqrt{h}$] is given in Table 2. The *w* value is given for two directions, as well as the water absorption in weight percent. The *w* value can be used to classify rocks into three types: (1) slightly absorbing [$w < 0.5$ (kg/m^2*$\sqrt{h}$), (2) medium absorbing (*w* 0.5–3.0 kg/m^2*$\sqrt{h}$), and (3) highly absorbing [$w > 3.0$ (kg/m^2*$\sqrt{h}$)]. According to this classification, most of the analyzed varieties are medium absorbing. Only the samples of Noyemberyan, Villarlod and Baumberger show a higher *w* value of > 3.30 [kg/m^2*$\sqrt{h}$] in the *X*-direction. Regardless of the samples, it should be noted that the capillary water uptake occurs relatively fast and is finished within the first 60–180 min. The saturation coefficient *S* describes how

Table 2 Petrophysical properties of the investigated tuffs and sandstones

Sample	BP	CV	LOS	BS	NB	GAF	VLj	BB	SA	SR
Porosity ([vol%)	14.9	29.5	16.8	14.9	25.7	21.5	19.5	24.3	15.4	15.0
Bulk density (g/cm^3)	1.85	1.54	2.07	2.06	1.73	2.04	2.17	2.03	2.27	2.30
Matrix density (g/cm^3)	2.17	2.18	2.49	2.42	2.34	2.60	2.69	2.68	2.68	2.70
Water absorption (wt%)	7	16	7	6	13	7	9	6	6	5
Saturation coefficient S	0.86	0.85	0.81	0.83	0.87	0.64	0.71	0.73	0.76	0.79
Micropores (%)	79	88	85	90	37	47	12	28	41	47
Capillary pores (%)	21	12	15	10	63	53	88	72	59	53
Mean pore radius (µm)	0.05	0.04	0.04	0.03	0.14	0.11	0.08	0.03	0.18	0.11
Pore radii distribution	uni	bi	bi	bi	uni	bi	uni	uni	bi	bi
SSA (m^2/g)	17	26	12	8	3	6	2	7	3	2
CEC (meq/100 g)	12	6	5	9	9	3	4	4	3	2
w-value (kg/m^2$\sqrt{h}$)										
X	0.8	2.8	0.8	0.8	3.9	2.6	10.7*	3.3	1.9	1.9
Z	0.8	2.6	0.7	0.5	3.8	2.7	8.43	3.2	2.0	1.8
μ-value							14.4 +	25**		
X	11.9	9.2	27.9	14.4	14.4	14.5	–	–	22.6	22.3
Z	11.1	10.1	13.4	14.2	14.5	14.5	–	–	27.9	26.2
Sorption 95% RH (wt%)	4.5	7.9	2.9	2.9	3.5	1.3	1.0 +	–	1.4	1.5
Hydric exp. (mm/m)										
X	0.71	1.39	0.58	0.35	0.67	0.39	1.70	0.60	0.5	0.5
Z	0.96	1.68	1.22	1.57	0.76	0.59	1.21	0.15	1.0	1.2
Mean	0.83	1.53	0.90	0.96	0.71	0.49	1.45	0.37	0.75	0.85
Dyn. Young's Modulus (Gpa)										
X	20	11	28	31	17	15	14 + +	19	33	33
Z	19	10	16	20	18	15	13.2 + +	–	32	32

uni unimodal, *bi* bimodal, *BP* Blanca Pachuca, *CV* Cantera Verde, *LOS* Loseros, *BS* Blue Sevan, *NB* Noyemberyan, *GAF* Golden Armenia Fine, *VLj* Villarlod jaune, *BB* Baumberger, *SA* Sander, *SR* Schleerieth

**w*-value determined by Tiennot et al. (2016); ***µ*-value for Baumberger determined by Visser and Mirwald (1998); + μ-value and sorption determined by Rousset and Bläuer (2009); + + dyn. Young's Modulus values determined by Tiennot et al. (2019)

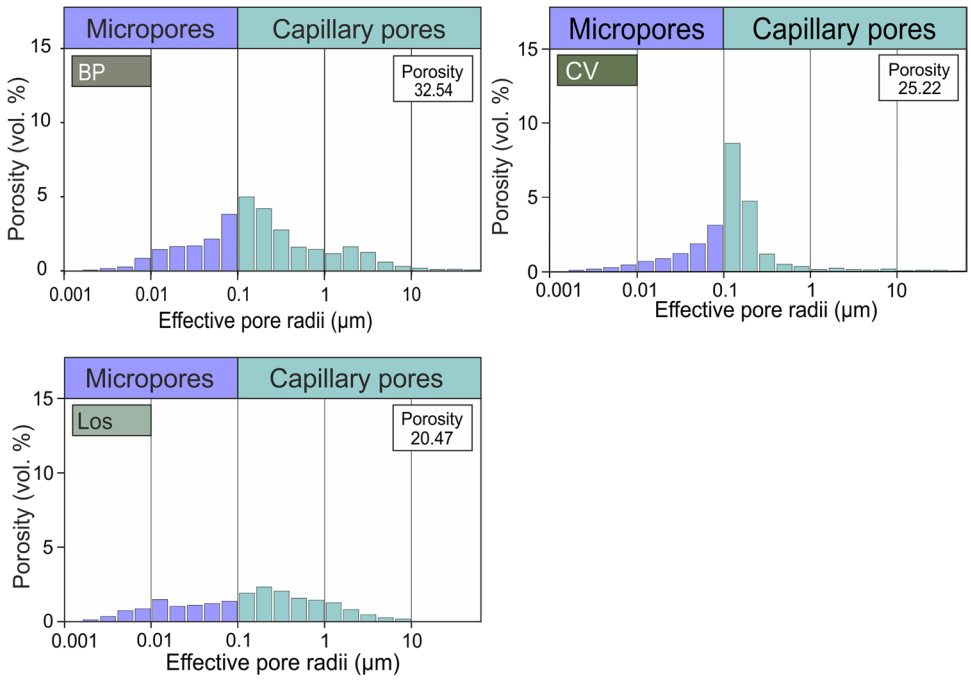

Fig. 7 Pore radii distributions for the Mexican tuffs Blanca Pachuca, Cantera Verde and Loseros

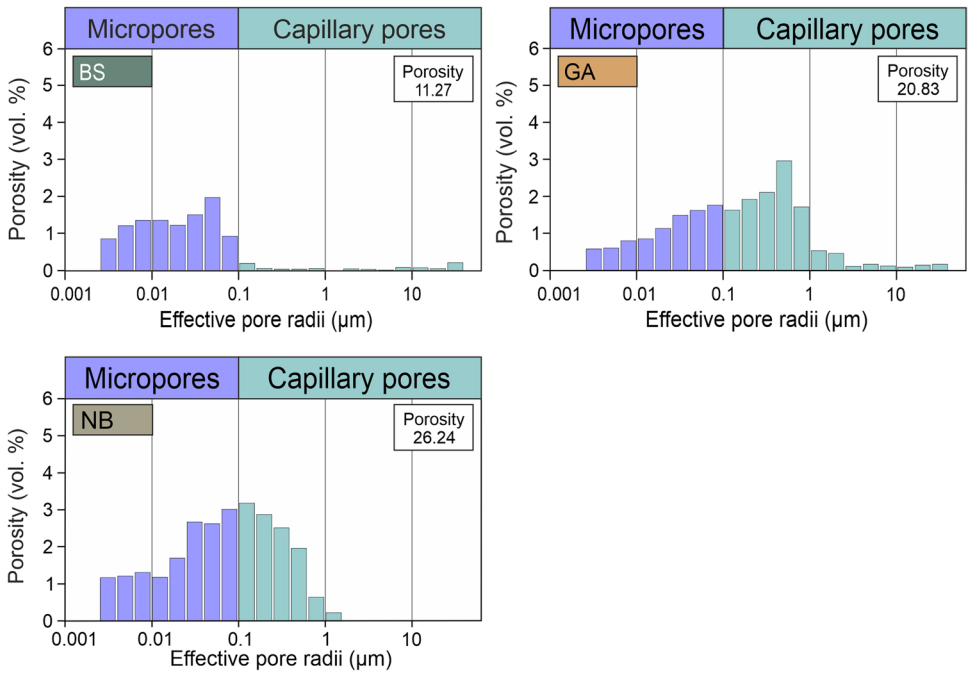

Fig. 8 Pore radii distributions for the Armenian tuffs consisting of Blue Sevan, Golden Armenia Fine and Noyemberyan

much of the total pore space is accessible to water absorption and helps to determine the frost resistance. Siegesmund and Dürrast (2014) describe that for metamorphic rocks, the saturation coefficient has limited significance due to the very small water absorption values under atmospheric and under vacuum conditions. They are influenced by the measurement procedure, the standard deviation of different samples, and the resolution limit. According to the classification of Hirschwald (1912), *S* values below 0.75 stand for a weather and frost resistant rock, while values below 0.9 indicate a rock which is not frost and weather resistant. From the analyzed samples, only Golden Armenia Fine, Villarlod and the Baumberger show values below 0.75, while all other samples exhibit higher *S*-values (Table 2).

The expansion measurements determined for Blue Sevan, Schleerieth and Sander in the *Z*-direction differ due to the heterogeneity of the rock material (see Figs. 10, 11, 12, 13 and 14). The hygric swelling and shrinkage

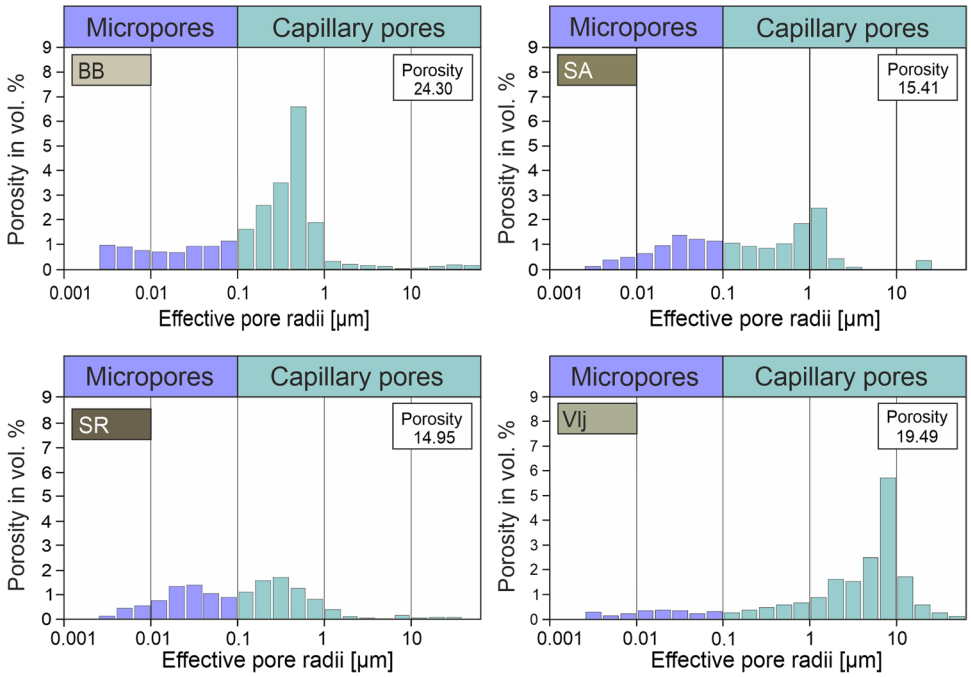

Fig. 9 Pore radii distributions for the sandstone samples comprising the Baumberger, Sander, Schleerieth and Villarlod jaune

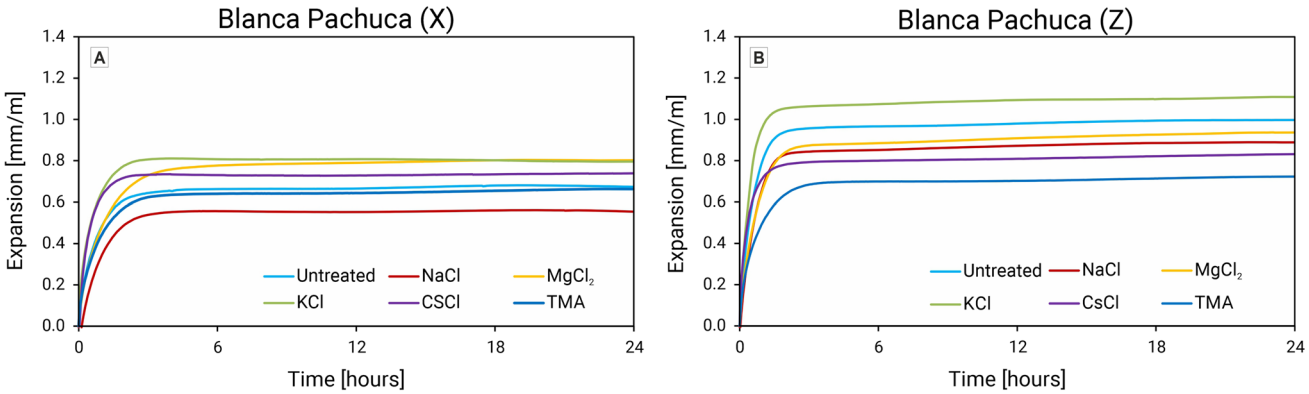

Fig. 10 Hydric expansion of Blanca Pachuca in the Z-direction and X-direction, treated and untreated samples

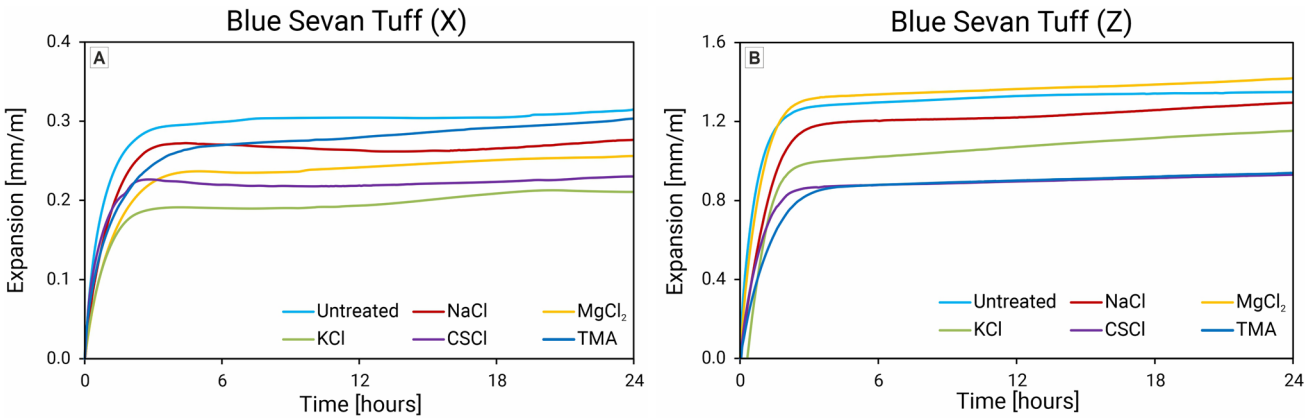

Fig. 11 Hydric expansion of Blue Sevan in the Z direction and X direction, treated and untreated specimens

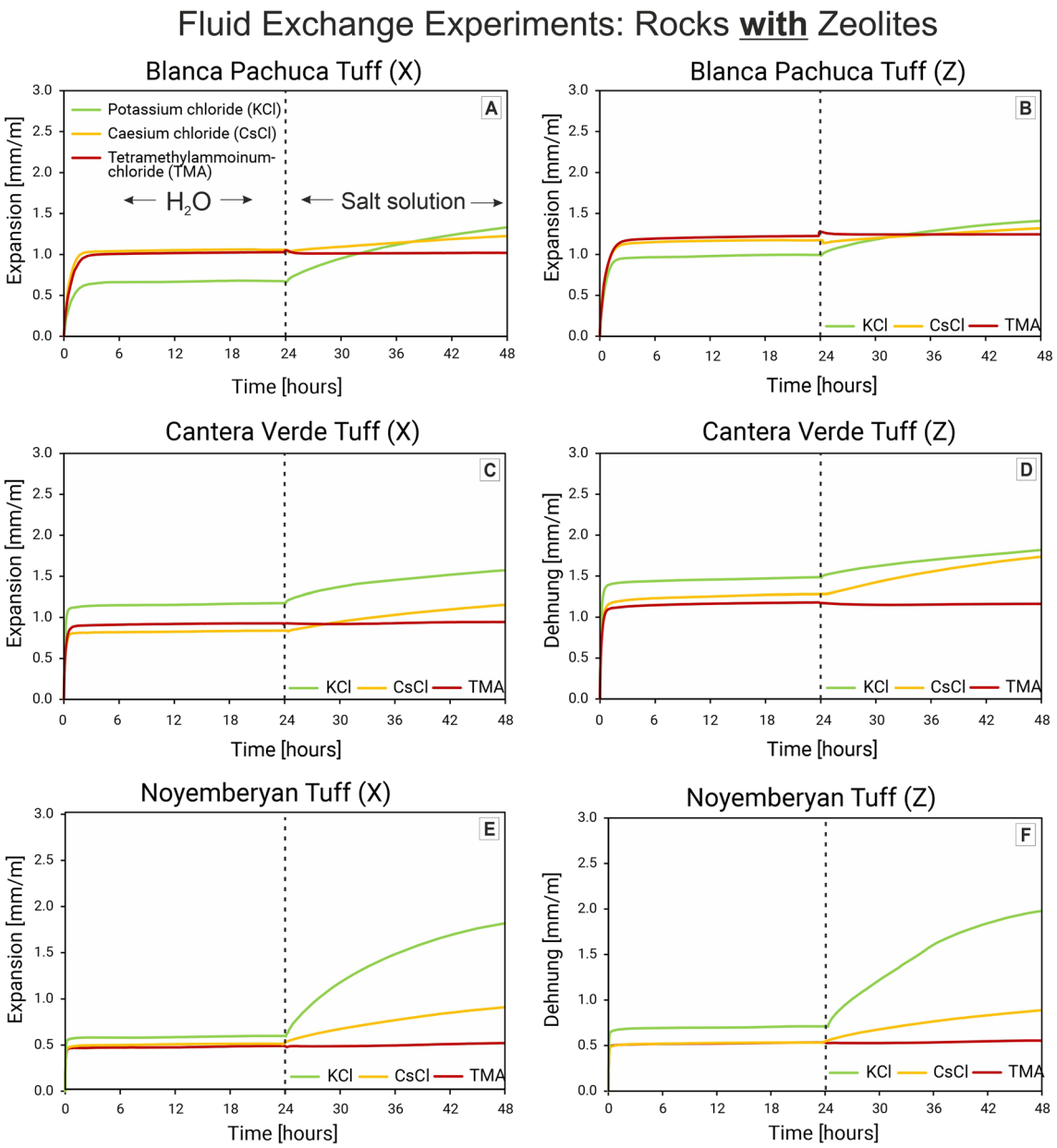

Fig. 12 Fluid exchange experiments in tuff samples from Armenia (NB) and Mexico (BP, CV) containing zeolites

behavior is related to the hygric properties of the rocks. The swelling values obtained on representative samples were investigated as a function of time and are given in Table 2. The Cantera Verde and the Villarlod show the highest values for hygric expansion with > 1.65 mm/m (Table 2). The expansion over time is different for each rock.

In a rock sample, the amount of extension differs between the different directions and the previous treatment of the samples. The hydric strain of Blanca Pachuca (Fig. 10), for example, is characterized by a moderate strain rate compared to the other samples, as well as an overall strain of about 1.00 mm/m in the *Z* direction and 0.68 mm/m in the *X* direction (Table 2). Blue Sevan shows a clearly anisotropic swelling behavior with strain amounts of 1.35 mm/m in the *Z* direction and 0.31 mm/m in the *X* direction (Table 2 and Fig. 11).

Overall, the determined swelling values for all samples (Table 2) vary between 0.35 mm/m for the Blue Sevan in the direction perpendicular to the layering (*X* direction) and 1.68 mm/m for the Cantera Verde in the *Z* direction. For almost all samples the values in the *Z* direction are significantly higher.

Swelling after cation pretreatment

To identify the mechanisms active during the hydric expansion, different swelling experiments were performed that proved to be useful for the identification of the primary swelling mode in clay-bearing sandstones (Wangler and Scherer 2008; Pötzl et al. 2018a). Figures 12, 13 and 14 shows the influence of impregnation with different salt solutions on the specimens. In almost all samples, hydric elongation is increased or decreased compared to the initial state. A clear trend with respect to the effect of the impregnation can only be seen with sodium chloride, as long as no zeolites are present. All samples impregnated with CsCl show reduced expansion compared to the initial condition. Both magnesium and potassium chloride have no consistent effect on the rocks.

The Blue Sevan, Loseros and Golden Armenia Fine samples (being free of zeolites) behaved largely as expected (Fig. 13A–F). While magnesium causes almost no change, the potassium leads to reduced swelling behavior (in Loseros only in the *X* direction). The fluid exchange confirms the effect of potassium. As described in Wangler and Scherer

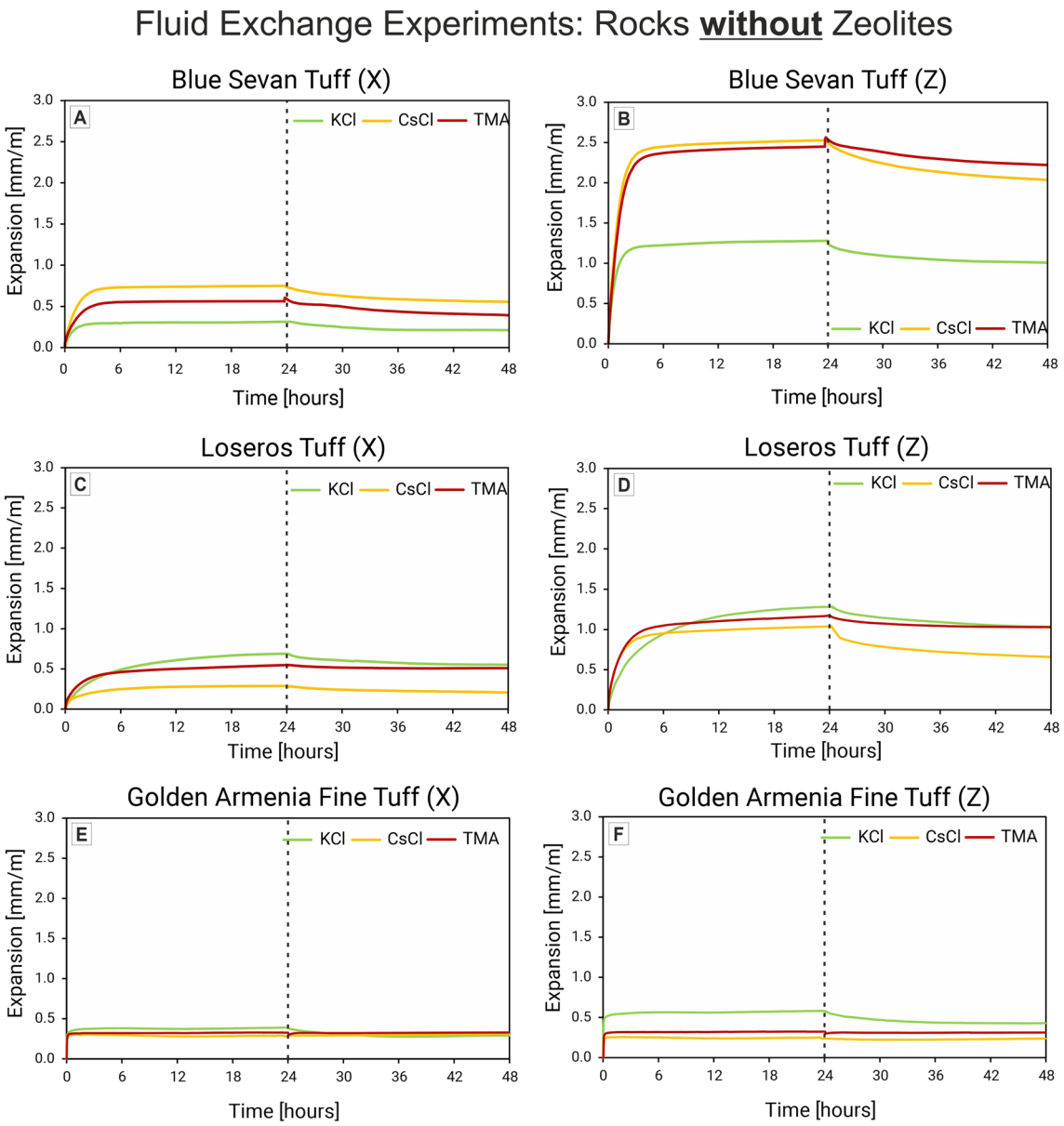

Fig. 13 Fluid exchange experiments for the Armenian tuffs Blue Sevan and Golden Armenia Fine and the Mexican tuff Loseros that contain no zeolite minerals

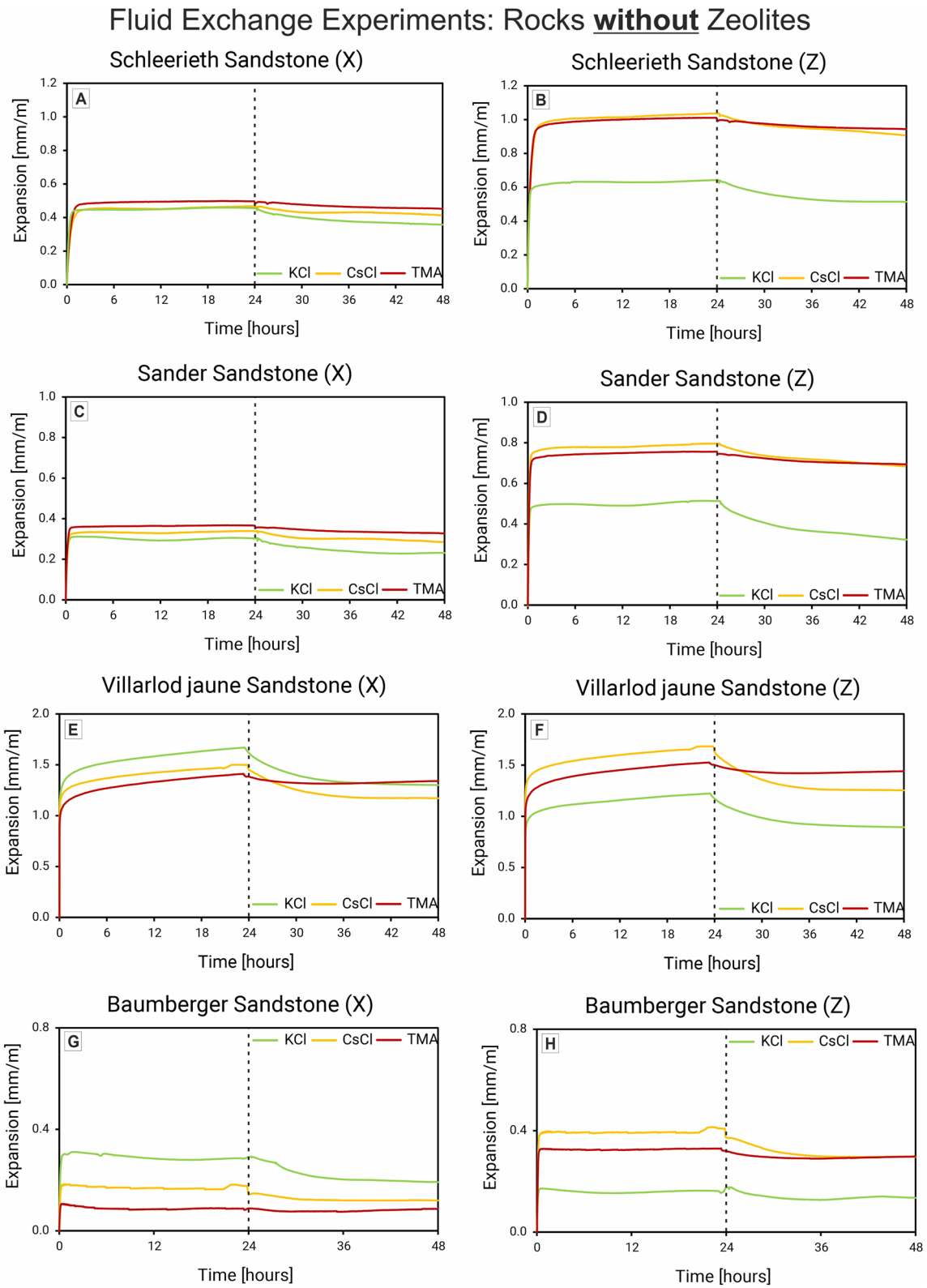

Fig. 14 Impregnation tests using KCL, CsCl and TMA in the investigated sandstones

(2008), the change from H_2O to potassium chloride solution (1 M) reduces the expansion by replacing water molecules with potassium cations in the clay mineral interlayers. This causes contraction of the specimens, which begins immediately after the fluid exchange. The samples Blanca Pachuca, Cantera Verde and Noyemberyan, all containing zeolites, behave in opposite ways regarding the influence of potassium (Fig. 12A–F). Cesium leads in both directions in Blanca Pachuca to a decrease of the extension, potassium to an increase. Magnesium leads perpendicular to the layering to a decrease of the expansion, whereas parallel to the layering an increase (Table 2; Fig. 12A, B). The fluid exchange after 24 h causes an expansion of about 0.4 mm/m with a slow expansion rate (Fig. 12).

Potassium causes increased expansion in these samples compared to the untreated samples. Fluid exchange confirms this behavior. Immediately after fluid exchange, the specimens begin to expand. In the case of the Noyemberyan tuff (Fig. 12E, F), even with higher, additional amounts of expansion was observed within 24 h. Moreover, the swelling behavior was not yet completed even 24 h after fluid exchange. In contrast, the main phase of contraction for the aforementioned specimens takes place immediately after fluid exchange and comes to a complete stop after 10 h at the latest. What becomes noticeable is that, in contrast to samples with small amounts of swellable clay minerals (a few wt%), the zeolitic samples contain approximately 30–50 wt%. So half of these tuffs are dominated by minerals of the zeolite group being able to significantly react on salt solutions by cation exchange.

The TMA shows a similar behavior in almost all specimens, i.e. there are no changes due to the addition of the TMA. Only for the Baumberger sandstone and the Villarlod is a slight reduction of the hygric strain observable (Fig. 14E–H). A comparable observation can be seen with the addition of CsCl (Cs^+ is larger than Na^+). Only in the rocks containing zeolites is there a slight increase in hygric strain due to the addition of the CsCl.

The hydric strain of the untreated specimens was first measured in distilled water for 24 h in these tests. Then, while the measurement was running, the water was exchanged for a one-molar salt solution. After 24 h with the salt solution, the measurement was terminated after a total of 48 h.

The difference in the behavior of the zeolite-free and zeolite containing samples with respect to a treatment with potassium can be explained on the basis of the unit cell volumes of the zeolites containing different cations. For that purpose, additional experiments have been performed on pure zeolite samples. The effect of ion exchange on the unit cell volume of two zeolite samples mordenite, $Na_{7.6}[Si_{40.4}Al_{7.6}O_{96}] * \times H_2O$ and clinoptilolite, $Na_{0.6}K_{1.8}Mg_{0.4}Ca_{1.3}[Si_{29.3}Al_{6.2}Fe_{0.5}O_{72}] * \times H_2O$, were analyzed using aqueous solutions of NaCl, KCl, $MgCl_2$ and $CaCl_2$. One gram of sample was stirred at 60 °C in 100 ml of a 1 molar salt solution. After 1 h the solution was removed and fresh salt solution added. In total, this was repeated six times. Subsequently, the samples were washed three times with distilled water and dried in open vessels at room temperature. XRD powder diffraction data were recorded using a Panalytical Empyrean powder diffractometer in Bragg–Brentano geometry and using Cu K-alpha radiation. Silicon powder was used as an internal standard. The unit cell volumes before and after the ion exchange were determined by Rietveld refinement.

The compilation of data in Table 3 shows that potassium can be completely exchanged for Na^+ in the case of mordenite and can be exchanged for Na^+ and Ca^{2+} to a very high extent in the case of heulandite. Potassium is a cation which is preferred over the other cations by the zeolites tested here. In contrast, sodium, magnesium and calcium can only partly replace the cations which are present in the original zeolites (synthetic Na-mordenite and natural heulandite).

Considering the differences in unit cell volume, the Ca^{2+} exchange leads to a slight shrinkage of the unit cell while the exchange using Na^+ or Mg^{2+} containing solutions has hardly any influence on the unit cell volume. The exchange with K^+ cations, however, leads to a considerable expansion of the zeolites. The observed expansion of rock samples by a treatment with K^+ containing solutions as presented in Fig. 12A–F can be explained by the above mentioned change of the unit cell volumes of the two zeolites. The zeolite content determined using the Rietveld refinement is approximately 30–50% in the samples Blanca Pachuca, Cantera Verde and Noyemberyan, with the highest mordenite concentration in NB (30 wt%), followed by BP (10 wt%) and CV (5–10 wt%). A hydric expansion of about 0.6–1.3 mm/m when treated with potassium containing solutions can be assigned predominantly to the expanding zeolites in the samples.

Although it is likely that the layered silicates, as well, exchange their cations to a certain extent, it seems that an ion exchange of the fully expanded layered silicates (after 24 h of exposure to distilled water) only leads to a slight change in volume. This becomes apparent when looking at the expansion curves of the zeolite-free samples displayed in Figs. 13A–F and 14A–H.

Discussion

To identify the primary cause of the moisture expansion due to swelling, swelling experiments were performed and discussed with respect to the mineralogical composition, the rock fabrics and additional petrophysical properties. Clay minerals and zeolites that expand due to the influence of a

Table 3 Relation between chemical composition and unit cell dimensions of different mordenite (MOR) and different clinoptilolite/heulandite (HEU) samples

Zeolite	Chemical composition as determined by XRF measurements [wt %]							Formula	Unit cell	
	Na_2O	K_2O	MgO	CaO	Fe_2O_3	SiO_2	Al_2O_3	H_2O	Chemical composition per unit cell	Volume [Å^3]	Difference related to Na form
Synth. Na-MOR	5.9	0.0	0.0		0.1	61.4	9.6	23.1	$Na_{7.6}$ [$Si_{40.4}$ $Al_{7.6}$ O_{96}] * x H_2O	2778.6(2)	-
K-MOR	0.0	9.5	0.0		0.1	65.1	9.8	15.1	$K_{7.6}$ [$Si_{40.8}$ $Al_{7.2}$ O_{96}] * x H_2O	2801.9(3)	+ 0.84 %
Mg-MOR	2.0	0.0	1.9	0.3	0.1	62.2	9.4	23.7	$Na_{2.5}$ $Mg_{1.8}$ $Ca_{0.2}$ [$Si_{40.8}$ $Al_{7.2}$ O_{96}] * x H_2O	2779.4(3)	+ 0.03 %
Ca-MOR	1.8	0.0	0.0	3.7	0.1	62.4	9.5	22.6	$Na_{2.2}$ $Ca_{2.6}$ [$Si_{40.7}$ $Al_{7.3}$ O_{96}] * x H_2O	2772.0(3)	- 0.24 %
Natural HEU	0.6	2.9	0.5	2.4	1.3	56.4	10.2	25.7	$Na_{0.6}$ $K_{1.9}$ $Mg_{0.4}$ $Ca_{1.4}$ [$Si_{29.7}Al_{6.3}O_{72}$] * x H_2O		
Na-HEU	4.0	1.5	0.3	0.7	1.0	50.1	9.3	32.9	**$Na_{4.6}$** $K_{1.1}$ $Mg_{0.3}$ $Ca_{0.4}$ [$Si_{29.5}Al_{6.5}O_{72}$] * x H_2O	2104.4(4)	-
K-HEU	0.2	6.4	0.0	0.4	0.9	39.7	6.8	45.4	$Na_{0.3}$**$K_{6.2}$** $Ca_{0.3}$ [$Si_{29.9}Al_{6.1}O_{72}$] * x H_2O	2113.1(3)	+ 0.41 %
Mg-HEU	0.2	2.3	1.5	1.8	1.1	48.6	9.2	34.8	$Na_{0.2}$ $K_{1.8}$ **$Mg_{1.4}$** $Ca_{1.2}$ [$Si_{29.4}Al_{6.6}O_{72}$] * x H_2O	2104.1(3)	- 0.01 %
Ca-HEU	0.3	1.3	0.4	3.2	0.8	42.9	8.4	42.3	$Na_{0.4}$ $K_{1.2}$ $Mg_{0.4}$ **$Ca_{2.3}$** [$Si_{29.3}Al_{6.7}O_{72}$] * x H_2O	2102.6(4)	- 0.09 %

The estimated errors related to the XRF measurements are ± 0.3 wt % for SiO2 and Al2O3 and ± 0.1 [wt %] for Na2O, K2O, MgO, CaO and Fe2O3. The chemical composition per unit cell is rescaled to the number of oxygen atoms of the silicate framework. The amount of water is calculated as a difference (but also covers a varying adsorption of the X-ray beam due to different sample densities). The low iron content of the natural heulandite sample which obviously cannot be exchanged is due to an impurity.

high relative humidity or uptake of moisture play a significant and decisive role in the damage and deterioration of natural stones such as volcanic tuffs and sandstones. These damages can be expressed in a number of different ways (e.g., scaling, flaking) and depend on the fabric and mineralogical composition of the rock.

Mineralogically and microstructurally very complex rocks (e.g. volcanic tuffs) show very interesting phenomena that need to be understood. For comparison we also introduced sandstones. The general aim of this approach is to expand our knowledge of the physical weathering processes and the course of damage to sandstones and tuffs caused by hygrothermal stresses. It will be determined to what extent the rock structure, with special consideration of anisotropy and heterogeneity, controls the extent of rock destruction. The mineralogical composition and microstructural properties of selected natural stones have been recorded in detail and correlated with quantified data of hygric strain.

Hygric expansion and CEC

As discussed in Ruedrich et al. (2011), XRD quantification of small amounts of clay minerals is not easy (Moore and Reynolds Jr 1989) and the interpretation of intensity differences can be misleading. Meanwhile, the application of the Rietveld method is applicable when interstratified (so-called mixed layer) clay minerals are present (Ufer et al. 2012a, b). Intra-crystalline swelling or shrinkage of clay minerals is only possible with a smectitic character of the interlayer regions. Such a 'smectitic character' is caused by an intermediate layer charge density of the 2:1 structural units forming these minerals; for further details see e.g. Ruedrich et al. (2011). The CEC can be used to check plausibility of clay mineral quantification. Smectites have much larger CEC values compared to all other clay minerals, if methods are used that allow relatively fast extraction of cations not exceeding 1–2 h (Bache 1965) based on the results of Dohrmann et al. (2012). Problems arise if "complicated CEC mechanisms" play a major role for certain minerals such as vermiculite (Weiss 1958) or the minerals of the zeolite group, e.g. (Barrer and Klinowski 1972) with very large selectivity differences compared to clay minerals (van Bemmelen 1888).

Ruedrich et al. (2011) reported on the petrographical properties of different sandstone types and found that the clay mineral composition and CEC values help in understanding the damage processes of natural building stones. Particularly the occurrence of swellable clay minerals within the rock fabric, e.g., in clay-rich lithoclasts and on grain boundaries. These may be important because large surface areas are available (ca. 750 m^2/g) in the interlayer galleries of such swellable clay minerals and has a factor of at least 10 times higher than non-expandable clay minerals. The large surface areas in the interlayer galleries are actively

involved as reaction surfaces for hydration of cations, and two processes are typical and fast: (1) exchangeable cations present for charge deficit compensation of the 2:1 platelets of the clay mineral structures can be readily exchanged by any cation present in pore water solutions just depending on energetic differences of the exchange as a driving force, and (2) hydration and dehydration of exchangeable cations causing swelling or shrinkage. The swelling pressures of bentonites (smectite-rich clays with mainly swellable clay minerals) may reach values up to 20 MP depending of course on the density of the materials used and type of measurement (e.g. Sridharan et al. 1986, Pusch et al. 1995; summarized in Kaufhold et al. 2015). The swelling pressure can reach such large values because the platelets can swell perpendicular to the large basal planes of the phyllosilicates (parallel to the c-axis). This also causes significant shrinkage upon drying.

When zeolites come into play, swelling processes upon hydration of cations or cation exchange may also occur, however, expansion is very much lower as the minerals are tectosilicates which are characterized by very rigid T–O bonds distributed throughout all three dimensions. The total volume available for water may reach up to 50% in zeolites (Barrer 1978). Cation exchange is much more size specific as for swellable phyllosilicate clay minerals as the reactive site for cation exchange are "inside" the zeolite structure, and cations have first to enter the inner surface area via small openings (e.g. Pahlke 2012).

Cation exchange may also occur at many energetically and geometrically different sites (multi-site exchangers). Both effects result in a pronounced cation-specific ion exchange capacity of zeolites. This property is different to swellable clay minerals of the smectitic group and is highly

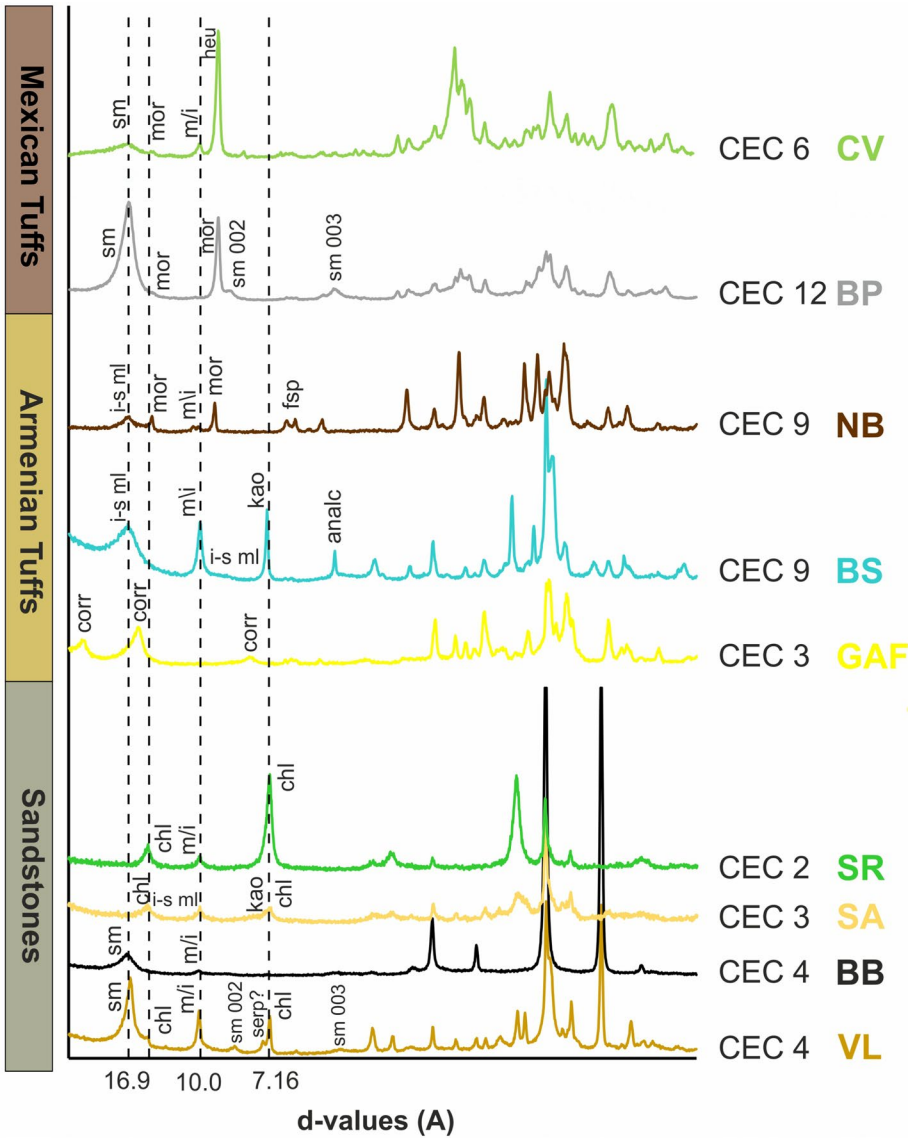

Fig. 15 XRD of clay fractions of the different rocks (measured as oriented mounts after EG intercalation): from top to bottom: Cantera Verde (CV), Blanca Pachuca (BP), Noyemberyan (NB), Blue Sevan (BS), Golden Armenia Fine (GAF), Schleerieth (SR), Sander (SA), Baumberger (BB), and Villarlod (VL). Note: Loseros (LOS) is missing as no material was left after testing to separate a clay fraction

welcome for technical processes using zeolites as "ionic sieves" in industry.

The sample set used in this study can be split into three groups with respect to relevant cation exchange and intracrystalline swelling processes, and applied to different kinds of sandstones and tuff rocks (see Fig. 15):

- Group 1 contains no swellable clay minerals and is represented by a single sandstone (SR).
- Group 2 contains swellable clay minerals (but no zeolites) and is represented by three tuffs (LOS, BS, GAF) and three sandstones (BB, SA, VLj).
- Group 3 contains zeolites either together or without swellable clay minerals and is represented by three tuffs (BP, CV, NB).

Group 1 includes the sandstone SR (Fig. 15) with no swellable clay minerals and the lowest CEC value of all samples (2 meq/100 g). This material should show the smallest effect on hydric expansion experiments.

Group 2 contains two samples with pure smectite as a swellable clay mineral (sandstones VLj, BB), and four samples with smectitic layers as part of the swellable interstratified clay minerals (tuffs LOS, BS, GAF, and the sandstone SA). In LOS, a small portion of pure smectite is present as well. With respect to swelling processes the reactive interlayer gallery volumes are believed to play the most significant role, no matter if these are part of an interstratified structure or not. Cation exchange and adsorption of hydration water around cations is a fast process and only limited by the amounts of accessible reaction volumes, not necessarily on the regularity of stacking sequences of these galleries in a crystal. The CEC values of group 2 are in the middle part of the CEC range of the sample set studied varying from CEC = 3–6 meq/100 g with one exception, the Armenian tuff (BS) with a larger CEC value of 9 meq/100 g.

Group 3 contains pure smectite as a swellable clay mineral (Mexican tuffs BP, CV) and the Armenian tuff (NB) with smectitic layers as part of swellable interstratified clay minerals. All these tuffs also contain zeolites: mordenite and heulandite/clinoptilolite. XRD quantification of whole rock samples allowed further differentiation into a mordenite-rich (30 wt%) tuff free of heulandite/clinoptilolite (NB), and heulandite/clinoptilolite-rich tuffs (35/30 wt%) with low amounts of mordenite (10/5–10 wt%; CV/BP). Tuffs present in group 3 contain the tuff with the largest CEC values of the sample set: BP (12 meq/100 g), followed by NB and CV (9 and 6 meq/100 g). As zeolites are size-selective cation exchangers, they may not contribute largely to the CEC determined with the large and colored CEC index cation Cu-triethylenetetramine (Cu-trien) used in this study (compare Meier and Kahr 1999). The authors found a CEC value of only 5 meq/100 g for pure clinoptilolite, whereas the same material adsorbed as much as 160 meq/100 g ammonium acetate, indicating the Cu-trien is too large to reach the inner volume of the zeolite minerals.

Within group 3 the cation exchange of water entering the tuff has a more complex way to react than in group 1 and 2 materials. Here some cations in such pore solutions for example may preferentially be adsorbed to a zeolite mineral as zeolites are, in contrast to swellable clay minerals, very specific cation adsorbers. Once such cations enter the inner volumes of zeolite minerals, hydrated cations being naturally adsorbed on exchange sites of cages or galleries in the structure, will be replaced by the entering cations and released into the pore solution. Accordingly, the chemistry of pore waters may change and this new equilibrium solution interacts with the cations adsorbed in the interlayer galleries of swellable clay minerals. Immediate cation exchange reactions may occur modifying again the pore water composition possibly causing a secondary cation exchange into the zeolites present. All cation exchange process come along with possible changes in volume, as described above. Such volume changes are relevant for hygric expansion processes.

The effect of the zeolites, however, on the hydric expansion of the samples Blanca Pachuca, Noyemberyan and Cantera Verde are of minor importance. At ambient conditions zeolites are nearly fully hydrated. The hydric expansion is generally very low compared to the intercrystalline swelling of smectites and related minerals. Mordenite and heulandite possess only a very limited capacity for hydric expansion. It cannot be excluded, however, that cations exchange between zeolites and smectites if water is present. This may influence the hydric expansion of the clay minerals.

The effect of zeolites and zeolite swelling

Zeolites are a group of minerals that can be described as crystalline aluminosilicates possessing a 3-dimensional silicate framework with micropores, which are occupied by inorganic cations like Li^+, Na^+, K^+; Mg^{+2+}, Ca^{2+}, Sr^{2+}, Ba^{2+} and water molecules. The framework is constructed from 4-connected $[SiO_{4/2}]$ and $[AlO_{4/2}]$ tetrahedra (Fig. 16). As an example, the formula of a natural clinoptilolite-type zeolite is presented here:

$$Na_{0.6}K_{1.8}Mg_{0.4}Ca_{1.3}\left[Si_{29.3}Al_{6.2}Fe_{0.5}O_{72}\right] * x\,H_2O(x = 0 - 24).$$

A characteristic property of zeolites is their ability to reversibly adsorb and desorb water depending on the temperature and the moisture level of the external environment. At ambient conditions, aluminosilicate zeolites are nearly fully hydrated. The percentage of water depends on the pore volume and the chemical composition of a zeolite and can amount up to 25 wt% of the hydrated

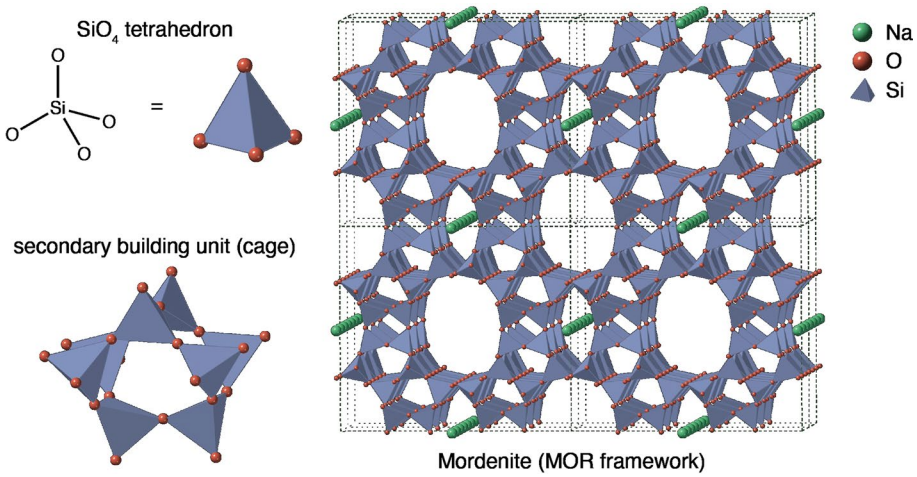

Fig. 16 The structure of clinoptilolite (slightly simplified drawing according to Koyama and Takeuchi 1977). Blue tetrahedra: [Si/AlO_4], light blue spheres: H_2O, other spheres: green (Na), red (O) and light blue (Si)

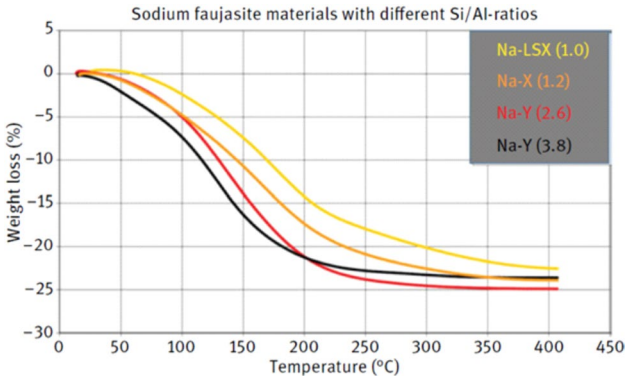

Fig. 17 A typical desorption curve of water from a zeolite with increasing temperature

mass. The water can completely be removed from the micropores in a continuous process by heating a zeolite up to about 350 °C. But even at, e.g. 50 °C, some water is lost compared to the water content at room temperature (see Fig. 17). Dehydrated zeolites, on the other hand, are strong desiccants. The cations like to form a symmetric coordination sphere of oxygen atoms—partly contributed by the silicate framework and partly by the oxygen atoms of the water molecules. Also, the polar aluminosilicate framework attracts water molecules. Because of strong Si–O and Al–O bonds the intracrystalline expansion and shrinkage of zeolites due to the uptake or loss of water molecules is limited to about 0.5% of the volume. This is in contrast to swellable clay minerals which may expand by values up to 20%. Moreover, different to layered silicates (clay minerals) the 3-dimensional tetrahedral framework of zeolites prevents strong anisotropic swelling. Zeolites will expand more or less equally in all three dimensions when changing the water content.

Another important property of zeolites is the cation-selective ion exchange capacity. The cations residing in the micropores (e.g., Na^+) can readily be exchanged against other suitable cations like K^+ if a zeolite is treated with a corresponding salt solution. A different charge, a different ionic radius of the exchanged cation and a different coordination sphere around this cation may also lead to an expansion or shrinkage of the zeolite. The difference in volume may vary between 0% and a maximum of about 1%.

Type, morphology, and localization of clay and zeolite minerals

Moisture-induced volumetric expansion of clay minerals leads to stresses at specific locations in the rock fabric. The locations where clay minerals can be found are in pore spaces, at grain contacts and along grain boundaries, forming along the edges of open microcracks, coating individual grains, or carpeting the grain fabric as in clay formation parallel the laminations or layering in the rock fabric. Similar localization aspects are also true for the zeolites investigated in this study. According to Ruedrich et al. (2011), however, when swellable clay minerals have formed in large macropores they have enough space to expand and the stone is less susceptible to being damaged.

The types of clay and zeolite minerals determined by XRD in the volcanic tuffs and sandstones are listed in Table 1. All tuff and sandstone samples were also investigated by SEM for localizing where the swellable and non-swellable clay minerals and minerals of the zeolite group occur. These are shown in Figs. 18, 19 and 20.

In all the Armenian tuff stones investigated (BS, GAF and NB) minor amounts of muscovite/illite occurs. Mixed-layer smectitic clays were determined in Blue Sevan (BS)

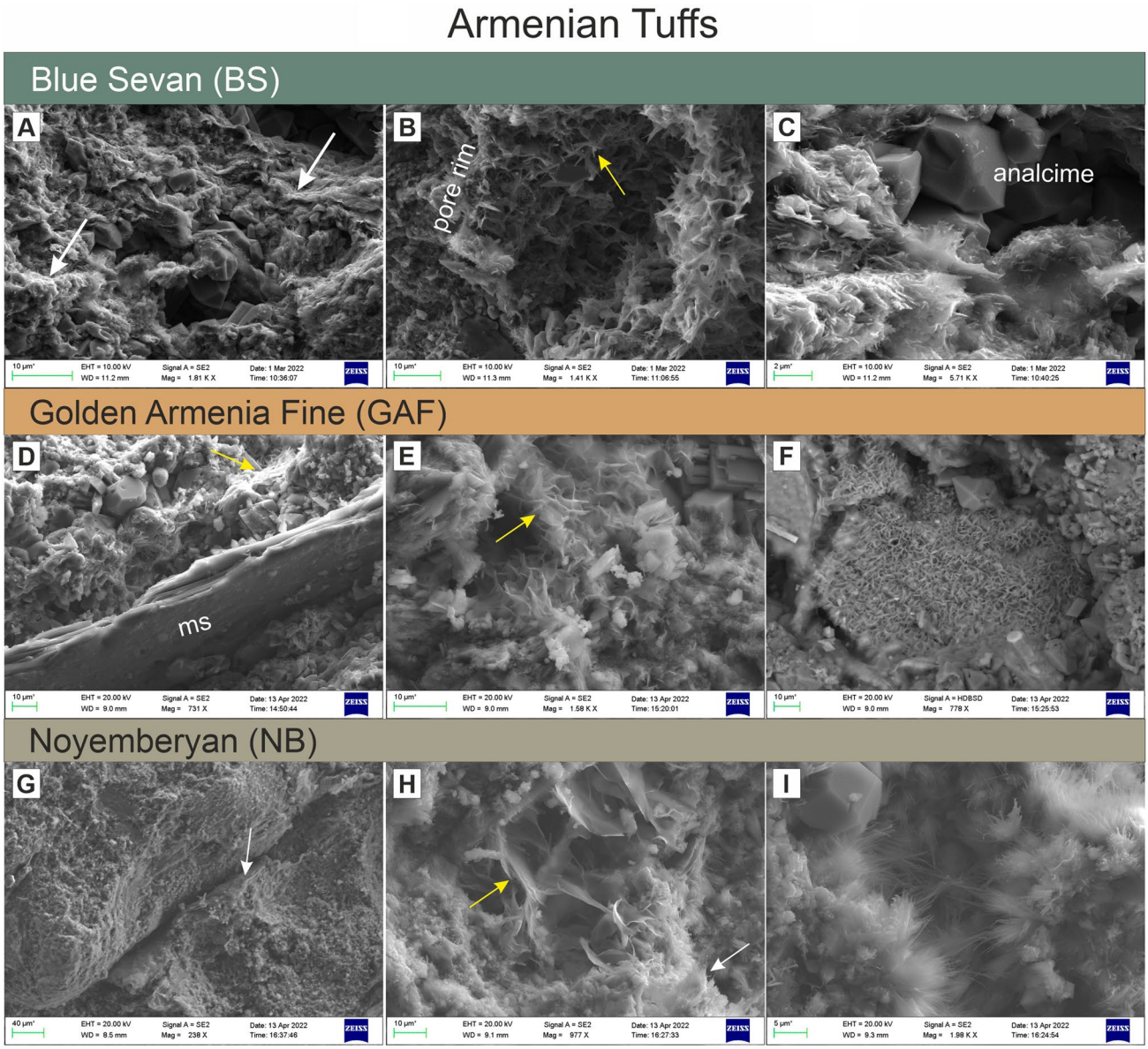

Fig. 18 SEM investigation of clay and zeolite minerals in the Armenian tuffs. **A–C** Blue Sevan, **A** close up of the structure of clay minerals (smectite mixed layer) parallel to the rock fabric consisting of altered glass, feldspar and euhedral analcime (white arrows), **B** pore space with smectitic mixed layer clay and needle-like illite (yellow arrow) coating the pore interior and the rim, and **C** close-up of a thick packet of smectitic clay minerals in the rock fabric along with euhedral analcime. **D–F** Golden Armenia Fine, **D** large muscovite flake (ms, foreground) showing open flakes with needle-like illite (yellow arrow) aligned parallel to the layering, **E** close-up of the mixed layer clay mineral corrensite (yellow arrow), and **F** corrensite coating a large pore space. **G–I** Noyemberyan, **G** open microcrack with a coating of dehydrated smectite mixed-layer clay (white arrow), **H** close up of smectitic mixed layer clay exhibiting the typical fence-like cornflake structure in a pore space (yellow arrow) along with accompanying fibrous mordenite (white arrow), and **I** open pore space containing fibrous needle-like mordenite

and Noyemberyan (NB), whereas the mixed layer corrensite mineral was found as the dominant clay mineral phase in Golden Armenia Fine (GAF).

In the Blue Sevan tuff (Fig. 18A–C), most of the swellable clay minerals form a carpet-like coating on the mineral surfaces, rather than being formed in larger pore spaces. They occur as coatings on plagioclase crystals. The mixed-layer smectitic clays are found penetrative throughout the rock fabric and aligned parallel to the very fine wave-like laminations consisting of a matrix of glass, quartz, K-feldspar and euhedral analcime (Fig. 18A). They are also located at grain contacts showing frayed edges, where they mainly occur parallel to the bedding plane (Pötzl et al. 2022). When the swellable clay minerals are

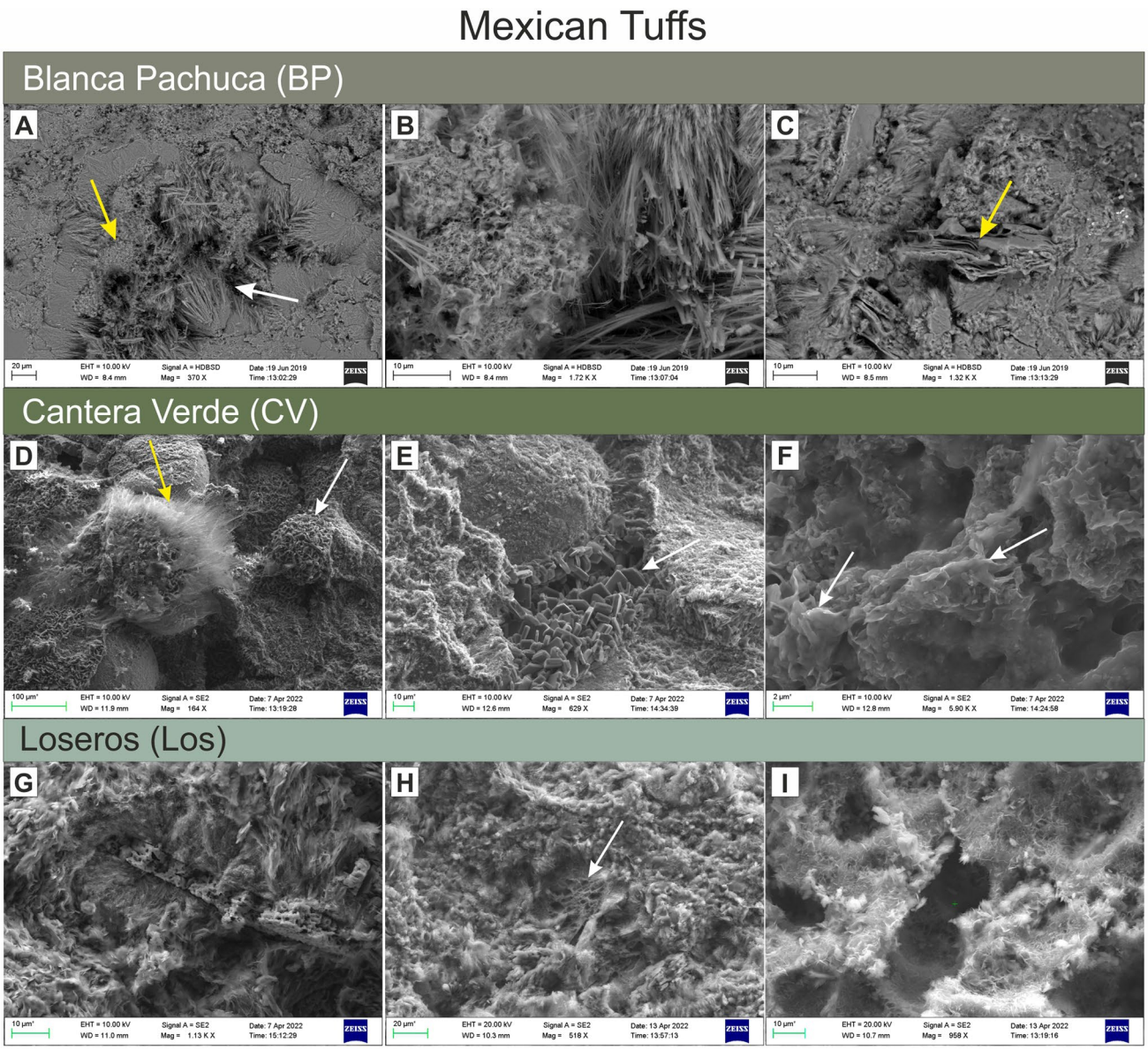

Fig. 19 SEM investigation of clay and zeolite minerals in the tuffs from Mexico. **A**–**C** Blanca Pachuca, **A** overview of rock fabric showing fibrous, needle-like mordenite (white arrow) and smectites (yellow arrow) in pore spaces and within the grain fabric, **B** close up of mordenite and smectite in a large pore opening, **C** bent and open smectite layers within the grain fabric (yellow arrow). Mordenite is also visible. **D**–**F** Cantera Verde, **D** fibrous mordenite (yellow arrow) attached to a grain with heulandite (white arrow) coating much of the grain fabric, **E** close up euhedral heulandite from the interior of a broken glass bubble (white arrow), **F** close up of smectite clay within the grain fabric (white arrows). **G**–**I** Loseros, **G** smectite and mixed-layer smectitic clays with slightly frayed edges penetrative throughout the grain fabric containing a strongly weathered feldspar grain (center), **H** clay minerals coating the grain fabric as well as an open pore space containing a unique fence-like clay mineral (white arrow), and **I** open pore space coated by mixed-layer smectitic clay

found in open pore spaces (e.g., in Fig. 18B), the complete pore space is coated with smectitic mixed-layer clays especially along the rim where they appear to be more frayed. Within the pore interior the clay minerals form a complex net-like structure with needle-like minerals (illite?) protruding into the open pore space.

In Fig. 18C a close up of the intracrystalline frayed edged smectites along with the associated analcime show the extent to which the Blue Sevan tuff has been altered, that leads to a delamination when the tuff is used as a natural building stone for monuments (e.g., the Blue Sevan constructed stele at the Odzun Church, Fig. 1B). According to Pötzl et al. (2022), areas of detachment are often associated with the frayed edge-like clay minerals, which have been determined to be intracrystalline swellable smectites. Needle-like or fibrous (illite or zeolite?) material is also observable throughout

the layered matrix of the Blue Sevan tuff. Large apatites and relics of weathered feldspar and muscovite can also be occasionally observed under the SEM.

Golden Armenia Fine (GAF; Fig. 18D–F) contains large amounts of clay minerals at grain boundaries and in open pore spaces. The clay minerals show a cornflake-like microstructure with frayed edges, but in contrast to BS and NB, the clay mineral in question is corrensite, a mixed layer, swellable chlorite-smectite and chlorite-vermiculite phase (see Beaufort et al. 1997). The SEM image in Fig. 18D shows that frayed corrensite occurs mainly parallel to the bedding and at grain contacts as defined by quartz, feldspar, glass and large muscovite flakes. Given their location along grain boundaries or at grain contacts, moisture expansion in the corrensite configuration would lead to expansion and breakage (Pötzl et al. 2022). At a closer magnification (Fig. 18E), corrensite shows the fence-like, cornflake structure with slightly frayed edges embedded in the tuff matrix especially at the grain contacts. In open pore spaces, corrensite can be seen coating the entire space as a complex fence-like structure (Fig. 18F). Moreover, a needle-like clay mineral, possibly non-swellable illite are also found parallel to the layering in some places. Devitrification processes and prismatic apatites as well as biotite and augite are also observable under the SEM.

The SEM/XRD investigation of the Noyemberyan tuff (NB; Fig. 18G–I) has shown that not only are mixed-layer smectitic clays prevalent throughout the rock fabric, but also mordenite of the zeolite group. Intracrystalline swellable clays are located on the inner surfaces of open microcracks as a coating (Fig. 18G, arrow). XRD identified these clay minerals as illite–smectite mixed layers. They occur as frayed minerals at the grain contacts parallel to the bedding plane and essentially carpet the entire rock fabric. Locally, the clay minerals occur in pore spaces (Fig. 18H) where they form complex fence-like structures with frayed edges at the pore rims.

Pervading the entire rock fabric are countless clusters of fibrous needle-like mordenite crystals. They crystallize out in almost all of the open pore spaces (Fig. 18I). These mordenite clusters grow out from the inner walls of the pore space. Non-swellable clays of muscovite/illite occur as a minor component according to the XRD analyses, where barite was also detected. According to Pötzl et al. (2022b), calcites and muscovites can attain dimensions of up to 300 µm.

The volcanic tuffs from Mexico (BP, LOS, and CV) all contain swellable smectite clay as identified by the XRD investigation (Table 1). On the other hand, zeolites consisting of mordenite and the heulandite/clinoptilolite pair were determined by XRD in Blanca Pachuca and Cantera Verde.

In Blanca Pachuca (BP), the SEM investigation has shown that fibrous mordenite needles grow out from the walls of pore spaces throughout the entire rock fabric (Fig. 19A, B). Smectite also occurs in close association with mordenite in some of these pore spaces with an almost clast-like appearance covering the mordenite (yellow arrow, Fig. 19A). These clay minerals form the typical cornflake structure and are shown in the SEM image of Fig. 19B. Smectite also occurs along the grain contacts as open and bent packets in the grain fabric (Fig. 19C). In general, the glassy matrix of Blanca Pachuca has been altered to clay and zeolite minerals (Pötzl et al. 2022).

The Cantera Verde (CV) tuff has a vitreous matrix that has been strongly altered to clay minerals consisting of smectite, muscovite/illite, chlorite and possibly kaolinite along with minerals of the zeolite group (mordenite and heulandite/clinoptilolite). Under the SEM, relict glass bubbles are visible which are altered to cristobalite, some of which still retain their rounded form. In Fig. 19D, the rounded glass bubbles (white arrow) are completely coated by euhedral heulandite crystals that also coat much of the grain fabric. A close up of the euhedral crystals are shown in Fig. 19E. Mordenite is strongly fibrous and shows a radial growth structure (yellow arrow, Fig. 19D). It grows out from matrix grains or relict glass bubbles into the open pore spaces. Moreover, mordenite has also been observed under the SEM growing out of the pits and cracks created in weathered feldspar grains. Smectite occurs in low amounts (with a CEC = 6). It occurs in the altered matrix at grain contacts, along grain boundaries (Fig. 19F), but also along the fractures in weathered feldspar grains.

The laminated Loseros tuff contains an abundance of swellable clay minerals consisting of minor smectite and mixed-layer smectites as the dominate phase. Minor amounts of non-swellable kaolinite also occurs. The mixed-layer smectites are aligned parallel to the laminations in the stone and penetrative throughout the rock fabric (Fig. 19G). Locally, smectite showing the fence-like structure can be found in some pore spaces (Fig. 19H, I) within the rock fabric carpeted by abundant clay minerals. Smectite is also found coating weathered feldspar grains.

Three of the sandstones (BB, SA and VLj) in the study contain swellable clay minerals consisting of smectite and mixed-layer clays. Only the Schleerieth (SR) sandstone was found not to contain any clay minerals as determined by XRD.

The Baumberger (BB) calcareous sandstone essentially shows a very fine-grained carpeting of the rock fabric by clay minerals (Fig. 20A). Large pore spaces are visible under the SEM as shown in Fig. 20B, where indications of clay minerals may be visible (yellow arrow), but are also difficult to discern. Even close-up imaging of the dominant calcite fabric shows little clay deposition in very fine pore spaces (Fig. 20C). The XRD analyses (Table 1) does indicate that smectite is a major component.

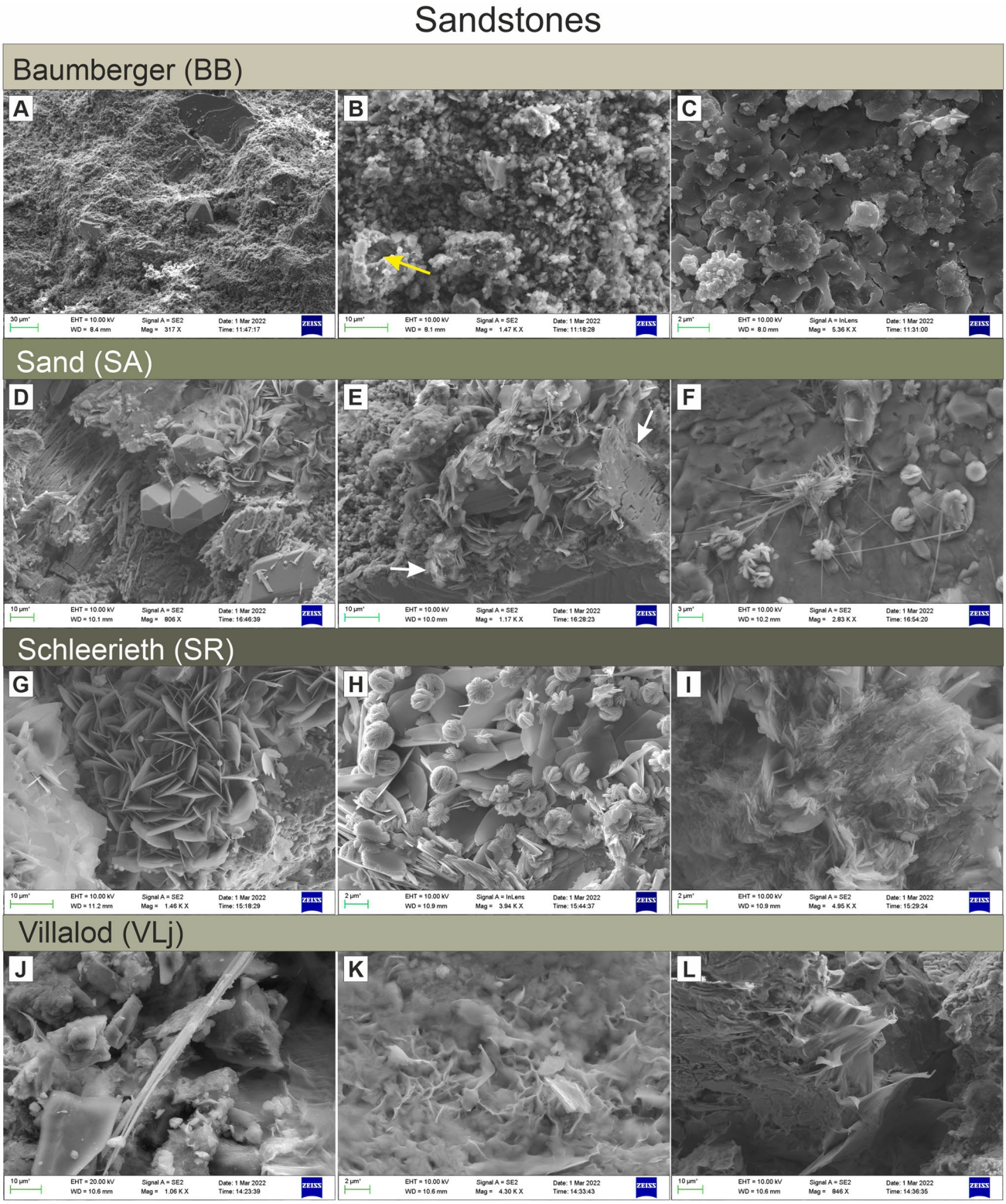

The SEM investigation of the Sander (SA) sandstone is shown in Fig. 20D–F. According to the XRD analyses, mixed layer clays are only a minor component, whereas the sandstone contains more non-swellable phyllosilicates consisting of muscovite/illite, chlorite and kaolinite. Chlorite occurs as two distinct phases: (1) as a Mg-rich platy shaped mineral or as an Fe-rich phase (chamosite) forming simple star-like structures that evolve into more complex rounded

◂**Fig. 20** SEM investigation of clay minerals in the sandstones. **A**–**C** Baumberger calcareous sandstone, **A** overview of clays carpeting the calcite-rich and quartz rock fabric, **B** pore spaces visible in the calcite rich rock fabric, **C** close up of the platy-like calcite and quartz. **D**–**F** Different phases visible in the Sander sandstone, **D** secondary euhedral quartz crystals with very fine-grained intergrowths of chlorite, **E** mixed-layer smectite clay and platy chlorite covering a weathered K-feldspar crystal; very small Fe-rich chlorite is also visible, **F** close-up of possible needle-like illite crystals and star-like rounded Fe-rich chlorites. **G**–**I** Distinctive chlorite mineralization and muscovite-illite (?) in the Schleerieth sandstone, **G** platy chlorite mineralization in a pore space, **H** distinctive rounded and star-like Fe-rich chlorite mineralization peppering the sandstone rock fabric, **I** possible swellable clay mineral (?). **J-L** Distinctive clay mineralization in the Villarlod sandstone, **J** lath-like illite and smectite in the grain fabric, **K** close-up of the cornflake-like smectite mineralization coating the rock fabric, and **L** frayed smectite mineralization in an open pore space

configurations. As shown in Fig. 20D, the platy chlorite forms as an intergrowth with secondary euhedral quartz and as clusters of platy minerals. This platy chlorite may also be associated with what is interpreted to be mixed-layer smectites forming a cluster around a weathered feldspar in the grain fabric (white arrows in Fig. 20E). Moreover, the intergrowth of this platy chlorite and quartz occurs throughout the rock fabric. Under the SEM, minor non-swellable illite (?) was found occurring as lath-like needles associated with the Fe-rich chamosite (Fig. 20F). Overall the fabric of the SA sandstone shows a fine-grained coating with chlorite and weathered and disintegrating K-feldspars.

Schleerieth (SR) is the sandstone that also contains both chlorite phases throughout the rock fabric. The SEM images are shown in Fig. 20G–I. Pore spaces are full of chlorite. Mg-rich platy chlorites occur as clusters in pore spaces or as intergrowths with quartz. The Fe-rich chamosite chlorites are also peppered throughout the rock fabric and are found in various stages of crystal growth (Fig. 20H). In the early stages, they appear star-like in structure in the free pore spaces and as growth continues they become more complex forming rounded shapes. According to the XRD analyses, no swellable clay minerals were detected, however, the SEM image in Fig. 20I does suggest the possibility of very minor amounts. These may be connected to the fact that in thin section the Schleerieth sandstone contains a high amount of lithic fragments, which may contain minor amounts of swellable clay minerals.

The Villarlod (VLj) sandstone variety contains smectite as the dominant swellable clay mineral and minor amounts of illite and chlorite. Illite occurs as a lath-like mineral in pore spaces (e.g., in Fig. 20J) and is estimated to make up around 5%. Smectite shows the typical cornflake-like structure within the grain fabric at grain contacts and in pore spaces (Fig. 20K, L). In pore spaces as in Fig. 20L, smectite shows frayed edges and under the high vacuum appears dry. Villarlod also contains carbonate phases consisting of calcite (dominant) and dolomite in the fabric. Many of the feldspars are visibly weathered when viewed under the SEM.

Clay minerals that expand due to the influence of a high relative humidity or uptake of moisture play a significant and decisive role in the damage and deterioration of natural stones such as volcanic tuffs and sandstones (see Figs. 1, 2). These damages can be expressed in a number of different ways (e.g., scaling, flaking) and depend on the fabric and mineralogical composition of the rock. As described above, clay minerals are located in pore spaces, at grain contacts, along grain boundaries, form along the edges of open microcracks, coat individual grains, or carpet the grain fabric parallel to the laminations or layering in the rock. Similar localization aspects are also true for the zeolites investigated in this study. The idealized sketches shown in Fig. 21 summarizes the location where clay minerals and zeolites are found in volcanic tuffs as well as where clay minerals occur in sandstones.

Modes of swelling

Different tuff varieties and sandstones were investigated for their petrographic and petrophysical rock properties, as well as their specific weathering behavior. The rocks differ mainly in their pore space properties and the type, amount and location of the clay minerals they contain (see SEM images in Figs. 18, 19, 20). These factors are of crucial importance, because the investigated hydric swelling processes are, as far as is known, either caused by intracrystalline swelling clay minerals or a cleavage pressure triggered by the interaction of surface forces at high micropore fractions in the nanometer range (Ruedrich et al. 2011).

To understand the effects of swellable clay minerals in more detail like smectites and their interaction with zeolites, additional synthetic samples were prepared to serve as model samples (Fig. 22). For these laboratory tests, cylindrical tablets (diameter 40 mm, height 10 mm) were pressed from powders. The various powder mixtures were either pressed into untreated tablets (blank) or previously soaked in 1-molar salt solutions for 48 h and then washed out with water before being conditioned. Since these model samples would not be stable in contact with water, their hygric expansion behavior was measured at 23.0 °C and 80% relative humidity. Prior to this, these samples were dried as much as possible in a drying oven at 105 °C.

The composition of the model rocks are pure mordenite powder (synthetically produced mordenite, see Table 3) with a composition of $Na_{7.6}[Si_{40.4}Al_{7.6}O_{96}]$ * ca. 24 H_2O, clinoptilolite with a composition of $Na_{0.6}K_{1.9}Mg_{0.4}Ca_{1.4}[Si_{29.7}Al_{6.3}O_{72}]$ * ca. 24 H_2O, and a Na^+

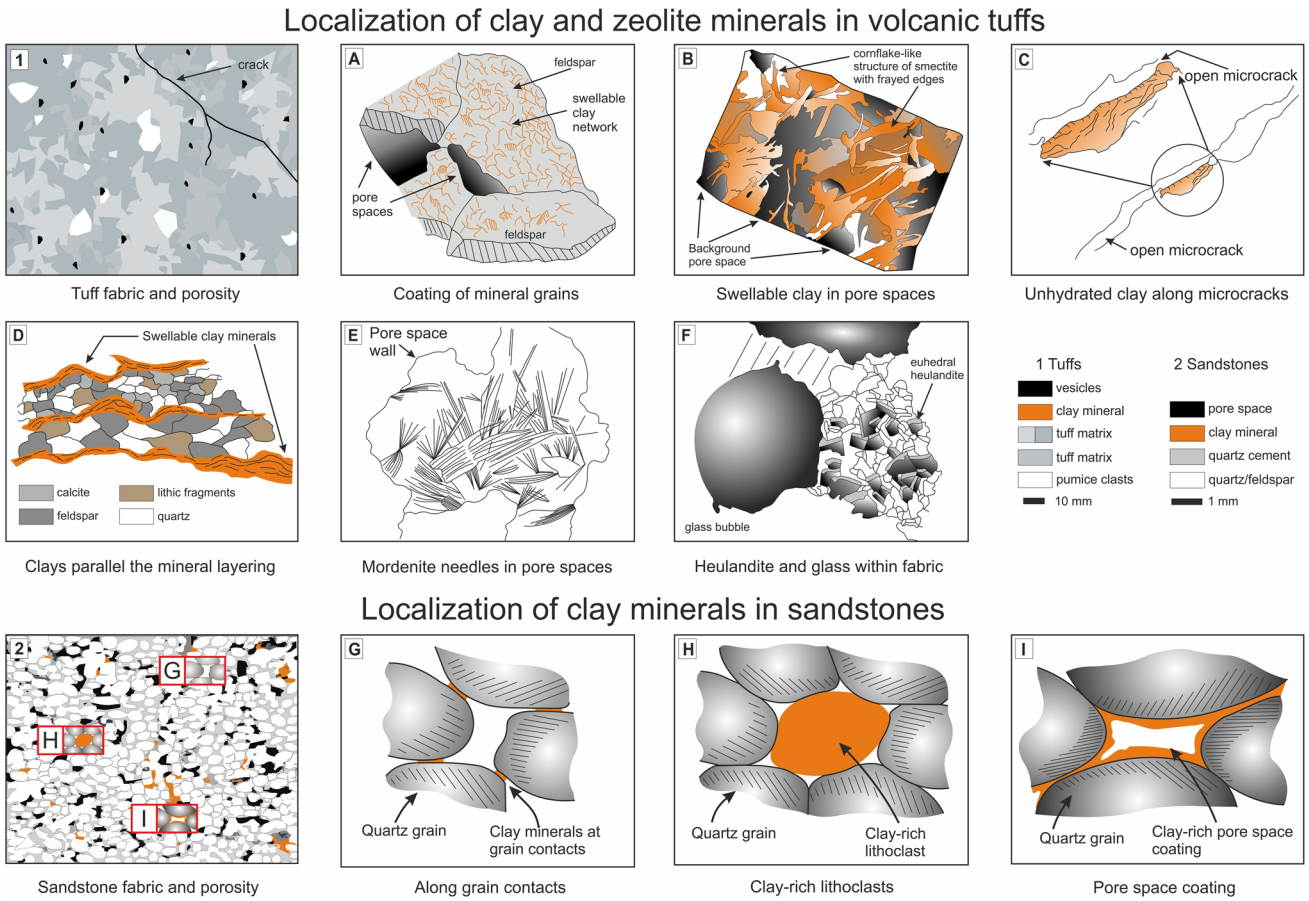

Fig. 21 Idealized sketches of the location of clay minerals and zeolites in volcanic tuffs and clay minerals in sandstones. **1** Generalized heterogeneous fabric of tuffs depicting vesicles and pumice clasts (modified after Cavazos-Álvarez et al. 2020). The matrix of tuffs can consist of volcanic ash, glass, quartz, feldspars, Fe-rich minerals and the weathering products thereof. The location of clays and zeolites are depicted in **A**–**F**. **A** Coating of mineral grains by a complex network of cornflake-like swellable clay minerals (e.g., smectite), **B** complex structures of swellable clay minerals with frayed edges in open pore spaces, **C** clays located along open microcracks, forming a coating of unhydrated clay draping over the crack edge, **D** in laminated tuffs clays form parallel to the bedding (e.g., the Loseros tuff, see Fig. 3F), **E** needle-like mordenite fibers are located growing out from the walls of pore spaces also in association with euhedral heulandite, and **F** euhedral crystals of heulandite within a fabric of volcanic glass bubble structures. **2** Sketch of a typical sandstone fabric showing porosity, the quartz/feldspar grain structure, clay minerals and quartz cement (modified after Farrell and Healy 2017). **G**–**H** shows where swellable clays in sandstones are located (after Ruedrich et al. 2011). **G** Along grain contacts, **H** as clay-rich lithoclasts, and **I** as a pore space coating similar to those in volcanic tuffs (e.g., a cornflake-like network of swellable clay with frayed edges)

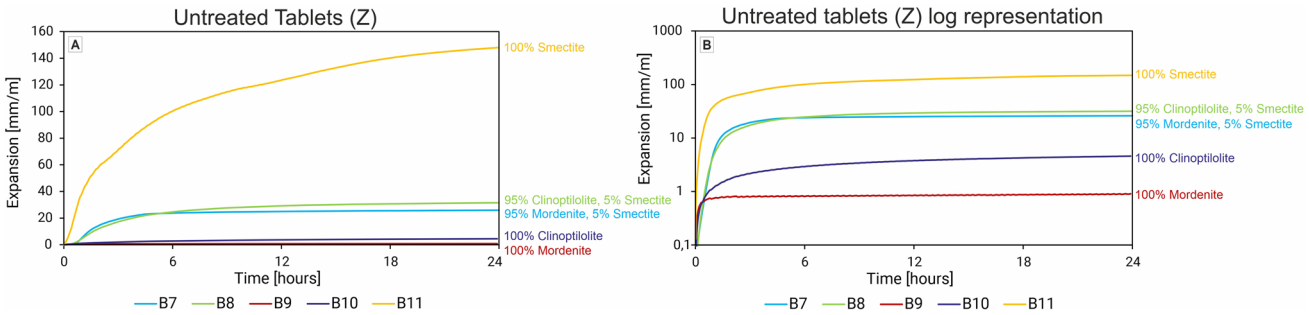

Fig. 22 **A**, **B** Graphs showing the limited capacity of mordenite and heulandite for hydric expansion in untreated tablets

-rich bentonite from Wyoming, USA (industrial product quality "Volclay SPV") with 84 wt% smectite, a CEC of 83 meq/100 g and 77% Na^+ cations on the exchange sites (sample #B27 in Dohrmann and Kaufhold 2010). In addition, synthetic mixtures with a portion of 5% bentonite (clay) and 95% clinoptilolite as well as 95% mordenite in each case were studied.

The hygric strain of the corresponding model specimens is shown in Fig. 22. The pure clay sample with 84 wt% of smectite shows strain values well above 140 mm/m, i.e. the model samples virtually collapse. The pure zeolite samples show the lowest strain values. Consequently, the corresponding zeolite/smectite mixtures exhibit hygric strains on the order of 20 mm/m. This 20-fold increase was caused by only a 4 wt% addition of smectite (5 wt% bentonite). This underlines the importance of swelling clay minerals with large intracrystalline surfaces on hygric expansion.

The CEC results for the tuffs and sandstones (see Table 1) are highly variable and very low for the sandstones, which is typical for these rocks used as building stones (see discussion in Ruedrich et al. 2011 or Pötzl et al. 2022). Only the Golden Armenia Fine shows a similar low CEC value (Fig. 23). All other tuff samples exhibit higher CEC-values from 4 up to 12 meq/100 g. The highest CEC of all fully swellable clay minerals determined is for smectites ranging from 70 to 120 meq/100 g (e.g. Weiss 1958, summarized in Bergaya et al. 2006). Micas, on the other hand, have the same structural TOT (2:1) units as smectites but a much higher layer charge density (1.0 charges per formula unit in contrast to 0.2–0.6 for smectites, Bailey 1980; Guggenheim et al. 2006). Accordingly, forces in the interlayer allow dehydration of K^+ cations, along with fixation centered above the di-trigonal holes of the tetrahedral sheet faced to the interlayer gallery. Such fixation in the large interlayer galleries causes a fully collapsed state of that region and a termination of any expandability (=non-swelling clay minerals). Such minerals only have cation exchange sites at the edges of the crystals and on outer basal surfaces of the crystals (a few dozens of TOT units form a crystal) exposed to the pore region with a low CEC (e.g. Weiss 1958). This limitation of CEC to edge sites is only similar to the non-charged (or nearly non-charged) clay minerals with formally 0.0 charges per formula unit such as talc or pyrophyllite, respectively. These minerals are coarser and have TOT (or 2:1) structures with Mg, respectively Al in the octahedral sheets. Also, the minerals of the kaolin group such as kaolinite with TO (or 1:1) structures have formally no layer charge along with low CEC values. In the case of the fine-grained dioctahedral and frequently occurring kaolinite, CEC ranges from 3 to 15 meq/100 g (Bergaya et al. 2006). CEC values for illite and chlorite were reported in the range of 10–40 meq/100 g (Grimm 1968). These minerals have much smaller particle sizes, which are equal to relatively larger edge surface areas. This explains their higher CEC values as compared to e.g. mica, however, as these reported values reach 40 meq/100 g, additional factors have to be taken into consideration. The problem with "pure illites", for example, is that they do not exist as reference materials in natural environments. If illite properties are reported in the literature, mostly this is impure illite (with a high layer charge of 0.6–0.9 charges per formula unit), but interstratified illite–smectite with different degrees of ordering. As a result of this fact, illites are defined as minerals which contain up to 5 wt% smectitic layers, the so-called ''frayed edge sites'' (Moore and Reynolds Jr 1989), which, together with much smaller particle sizes equal larger edge surfaces and explains their higher CEC values compared to e.g. mica.

Starting from this general consideration, the CEC should correlate very well with swelling strain. According to Fig. 23, however, there is no clear evidence that a high CEC value means a high swelling strain. If we take the average elongation values between 0.8—approximately 1.0 mm/m, these samples can differ in CEC value between 2 meq/100 g and 12 meq/100 g. If the directional dependencies are also taken into account, the Blue Sevan (BS) and the Cantera Verde (CV) show the highest strain values with > 2 mm/m. A particularly interesting example would be the Schleerieth sandstone with a very low CEC and the absence of swelling clay minerals (see Table 2; Fig. 20G–I). This was confirmed by the studies of Demarco et al. 2007; Ruedrich et al. 2011 or Grimm 2018. The Schleerieth sandstone also contains lithoclasts of volcanic and sedimentary rocks and two types of chlorites (see Figs. 6D, 15, 20G–I) as well as lesser amounts of muscovite/illite. These occur in the pore spaces as well as distributed throughout the rock structure. Obviously, the presence of expandable clay minerals with large reactive surface areas in interlayer galleries alone cannot explain the observed differences. The potential swelling ability and the actual strain caused by such swelling seem

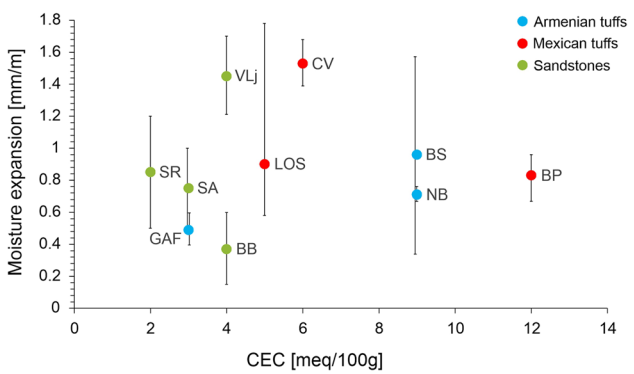

Fig. 23 Moisture expansion versus the CEC in all the tuff and sandstone samples investigated

to be independent and further factors have to be identified causing the observed differences.

As can be seen in Table 3 all cations (Na^+) can be exchanged (for K^+) in mordenite and nearly all cations (Na^+, Mg^{2+} and Ca^{2+}) for K^+ in clinoptilolite. Based on the chemical composition, the CEC values of

$$\text{mordenite,} Na_{7.6}\left[Si_{40.4}Al_{7.6}O_{96}\right] * \text{ca.24 } H_2O, \text{ and}$$

$$\text{heulandite,} Na_{0.6}K_{1.9}Mg_{0.4}Ca_{1.4}\left[Si_{29.7}Al_{6.3}O_{72}\right] * \text{ca. 24 } H_2O,$$

as used for the experiments presented in Fig. 22, are calculated to ca. 210 meq/100 g (or cmol/kg) and ca. 220 meq/100 g, respectively. In the literature, as well, values of around 200 meq/100 g are reported for the pure natural zeolites (see for example Filippidis et al. 2007).

To understand the mode of hygric expansion active during the swelling, additional experiments were performed for the identification of the swelling mode. Intracrystalline expansion is of particular importance for clay-bearing rocks due to the intercalation of water between the silicate layers of the crystals as discussed above. Kahr et al. (1986) calculated the swelling pressure that results from the attachment of the individual water layers for a pure montmorillonite. This process is also called hydration of the interlayer cations. For the formation of the first water layer the pressure is equal to 400 MPa, up to 110 MPa for the second water layer and up to about 27 MPa for the formation of the third and fourth layers. The hydration energy of the intermediate cation determines the exchange with the other cations.

As described by Wangler and Scherer (2008) and Pötzl et al. (2018a), swelling and shrinkage processes in rocks are mainly driven by the hydration and dehydration of exchangeable cations in the interlayer galleries of expandable clay minerals. Both studies showed that sodium and magnesium lead to an increase in the expansion, while samples treated with potassium showed a significantly lower expansion (Fig. 24). The influence of the cations was explained by the fact that these occupy the interlayer areas and promote (Na, Mg) or inhibit (potassium) hydration.

Four different sandstones have been selected that differ significantly in mineralogical composition and rock properties. The Baumberger calcareous sandstone and the Villarlod contain swellable clay minerals, namely smectite, the Sander has some swellable smectitic-mixed layers, whereas the Schleerieth sandstone has only non-swellable clay minerals (chlorite, muscovite and illite). The CEC values support the XRD results (Table 1; Fig. 15). The clays in the Villarlod and Baumberger sandstone samples exhibit the highest CEC, compared to the other two sandstones. They both have very low microporosity at 24.3 vol% * 0.28 = 6.8 vol%, relatively large amounts of swellable clay minerals and relatively little to no non-swellable clay. The Villarlod has a lower microporosity (19.5 vol% * 0.12 = 2.3 vol%, see Table 2 and Fig. 25) but up to < 10% clay minerals consisting of kaolinite, glauconites, chlorite, and especially smectite. According to Tiennot et al. (2016, 2019) and Wangler (2020), this should explain the very pronounced hygric swelling observable in this rock (see also Wangler and Aquilar Sanchez (2020)). The directional dependence of hygric swelling is a matter of anisotropy, i.e., rock structure or heterogeneity.

In the literature, a maximum value of 1.6 mm/m has been reported for the Baumberger sandstone (see Visser and Mirwald 1998 or Blöchl et al. 1998). This is in contrast to the measured hygric expansion values of max. 0.60 mm/m in this study (see Table 2). The significant variation is a result of the anisotropy or in parts due to the heterogeneity, with values varying widely when perpendicular to the layering. Furthermore, the mineralogical composition varies with the facies type in the Baumberger limestone (Kettelhack 1992; Visser and Mirwald 1998; Blöchl et al. 1998; Weiss et al. 2004). Facies types range from wackestone to packstone to biomicrites, which are glauconite-bearing, fine sandy

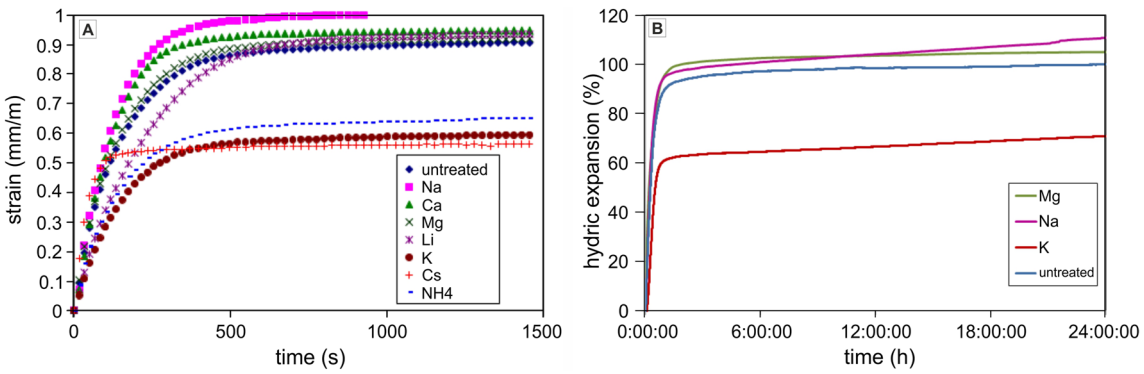

Fig. 24 **A** Hydric strain of Portland brownstone (sandstone; Wangler and Scherer 2008) and **B** the Hilbersdorf tuff (Pötzl et al. 2018a) under the influence of different cations and molecules, respectively

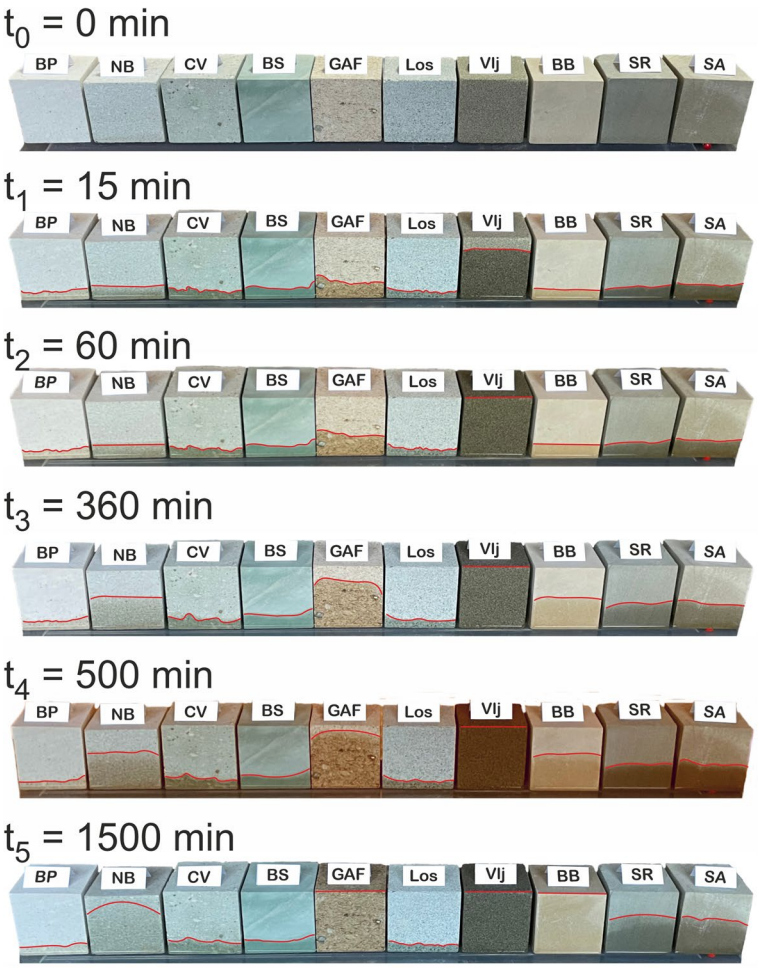

Fig. 25 Simple experiment for demonstrating capillary water uptake. The cubic samples of the study are placed in a tray of water over a specific time period. The diagram shows the water uptake at the initial dry condition ($t_0 = 0$ min) and at the intervals 15, 60, 360, 500 and 1500 minutes. Samples shown are: the tuff stones Blanca Pachuca (BP), Noyemberyan (NB), Cantera Verde (CV), Blue Sevan (BS), Golden Armenia Fine (GAF), Loseros (Los), and the sandstones Villarlod (Vlj), Baumberger (BB), Schleerieth (SR) and Sander (SA). Note the enormously fast water uptake of the Villarlod molasse sandstone at $t_1 = 15$ minutes and by $t_2 = 60$ minutes the stone is completely saturated. This demonstrates that the stone should only be used for interior purposes. By 1500 minutes, BB, GAF are also totally saturated with NB close to complete water absorption. Only the tuffs BP, CV, BS and Los show a much slower capillary water uptake. The red line represents the extent of the rising capillary water uptake front

clayey limestones with fossil particles and clayey micritic matrix (Kettelhack 1992). The Baumberger sandstone has no macroscopically recognizable layering but some carpeting of the clay minerals like smectite and some muscovite and illite (see SEM images in Fig. 20A–C). According to Kraus (1985), the Baumberger calcareous sandstone shows a high porosity and a high proportion of capillary pores as well as a large water capacity of 16 vol%. The good moisture adsorption capacity is proof of this (Fig. 25). According to these data and the results of Blöchl et al. (1998), it is clear that swelling is less related to moisture absorption in the micropores. Moreover, based on the pore radius distribution, it is clear that about 80% of the maximum water saturation is due to the filling of the capillary pores (see discussion in Kraus 1985, Fig. 25). In the presence of a 1 molar NaCl solution, an increase in elongation is shown, while the presence of 1 molar KCl solution leads to a reduction in hygric elongation (see Blöchl et al. 1998). This observation strongly suggests that intracrystalline strain should be the most important swelling process as K^+ intercalation leads to the contraction of the interlayer distances.

The Villarlod sandstone also shows a high CEC and a pronounced hygric elongation. The Villarlod is available in different gray-greenish, yellowish and bluish varieties. Our investigation was carried out on the yellowish variety (VLj), since the highest hygric elongation values were determined in this variety. The swelling values obtained on representative samples range from 1.21 to 1.70 mm/m. They depend on the direction in the rock (perpendicular and parallel to the layering). Tiennot et al. (2016) determined values for the hygric expansion of Villarlod of 0.48 mm/m and 0.27 mm/m perpendicular and parallel to the layering at a relative humidity of 25%. At 97% humidity, the hygric strain increases to 0.68 mm/m and 0.25 mm/m, respectively (Tiennot et al. 2016, 2019). Wangler (2016) determined maximum values of up to 1.83 mm/m swelling strain for the Villarlod, which corresponds to our strain values (Table 2). Ruedrich et al. (2011) was able to determine that hygric strain as a function of moisture exhibits a behavior that roughly corresponds to the relationship between the moisture expansion and the saturation degree. Between 35 and 75% RH, a fairly linear increase of length is observable. Only above 75% RH

a significant change in length was observed. As expected, all samples at 95% RH showed a smaller expansion than when measured saturated in water. Rousset and Bläuer (2009) were able to show that the hygroscopicity of the Villarlod grows comparatively constantly between 33 and 86% relative humidity and then suddenly increases between 86 and 97% relative humidity, which is certainly due to strong capillary condensation in the fine pores at above 86% relative humidity. This could suggest that swelling in Villarlod is not due to moisture uptake in the micropores but rather linked to water uptake in the capillary pores (Fig. 25). Capillary water absorption, a voluntary process due to capillary suction forces results in a *w*-value for the Villarlod of 7.7 [kg/m^2*$\sqrt{}$h]. Thus, the Villarlod belongs to the strongly absorbing rocks, which is documented by the very high proportion of capillary pores (Fig. 25). Our swelling measurements show that the final value is approximately reached after only 8–10 min. The water absorption under vacuum resulted in a value of 9.0 wt%. The swelling is lowered by cation pretreatments with 2 molar KCl and MgCL solutions, while 2 molar NaCl solutions increased the swelling (Wangler 2020). This corresponds to earlier results from Wangler and Scherer (2008), Ruedrich et al. (2011) or Pötzl et al. (2018a), where intracrystalline swelling is expected to represent the dominant swelling mode.

The Blue Sevan, Loseros and Golden Armenia Fine samples behaved largely as expected (Fig. 13). While Mg^{2+} cations causes almost no change, the potassium leads to reduced swelling behavior (in Loseros only in the X direction). Blanca Pachuca, Cantera Verde and Noyemberyan tuffs behave opposite to the first group. These three samples contain smectite and a higher amount of zeolites (Table 1, SEM images in Figs. 18G–I, 19A–E). Noyemberyan shows a higher amount of mordenite and some smectitic mixed layers. As far as the influence of potassium is concerned, this element causes an increased expansion in these samples compared to the untreated samples. The fluid exchange confirms this behavior. Immediately after fluid exchange, the samples begin to expand. In the case of the Noyemberyan tuff, this occurs with an even higher and additional amount of expansion (Fig. 12E, I). Moreover, the swelling behavior of this sample is not even complete after the fluid exchange. From this observation, it also seems to be obvious that for this sample intracrystalline swelling is the dominant mode of the hygric properties. The expansion of the zeolite containing tuffs Blanca Pachuca, Cantera Verde and Noyemberyan after fluid exchange (adding potassium) is due to the expansion of the unit cell of the zeolites when K^+ replaces the other cations which occupy the pores of the original zeolite materials (see Table 3 last column).

The mechanism of intercrystalline swelling was also tested. Intercrystalline swelling (or osmotic swelling) occurs when water accumulates on the outer surface of the crystals. This should be particularly strong for the platy clay minerals because of their larger surface area and less so for the more isometric crystals such as quartz, feldspar, calcite, etc. The criteria for this strain would be: small microporosity, high proportion of non-swellable clays and very low proportion (absence) of swellable clay minerals.

To prove the osmotic swelling the samples were also placed in distilled water. When full saturation was reached, the water was syringed out and replaced by a concentrated salt solution of about 1 M. As soon as the salt diffuses into the pore space of the rock, the water of the interlayer space or interparticle space would flow into the pore space to balance the concentration. Thus, an osmotic effect would result in a contraction of the stone. This causes contraction of the samples, which begins immediately after fluid exchange.

The zeolite-bearing tuffs (BP, CV and NB) for which no contraction was observed during the fluid exchange approach is essentially evidence that no osmotic strains were recorded. All other rocks show the existence of this hygric mode, i.e. osmotic swelling. Again, for the Blue Sevan, Loseros and Golden Armenia Fine fluid exchange confirms the effect of

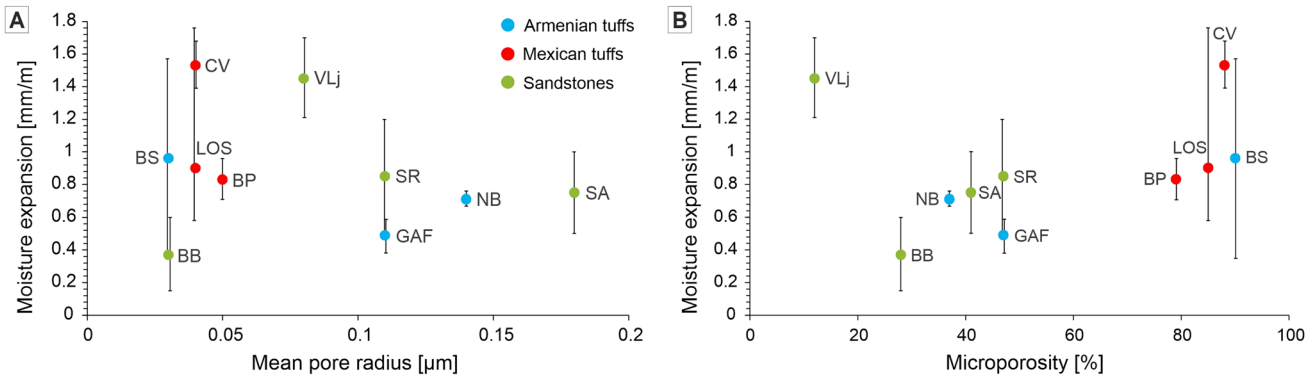

Fig. 26 Moisture expansion versus the mean pore radius (**A**) and (**B**) moisture expansion versus the microporosity in percent for the Armenian and Mexican tuffs and the investigated sandstones

potassium. As described in Wangler and Scherer (2008), the change from H_2O to potassium chloride solution (1 M) reduces osmotic expansion by replacing water molecules with potassium cations in the clay mineral interlayers (Fig. 12A–F). This causes contraction of the samples, which begins immediately after the fluid exchange. Minor contraction of less than 5% of the original swelling was observed for most of the investigated varieties. The effect of osmotic strain can also be observed for the sandstones. The amount of this hygric mode varies in intensity for the individual rocks and also depends on the rock fabrics (Fig. 26).

In the literature it has been shown that for various rocks, high hygric strain occurs even though no swellable clay minerals exist (see Ruedrich et al. 2011; Pötzl et al. 2018a). This mode, known as disjoining pressure, is significant for rocks that have a large microporosity (=porosity * micropore fraction), a low proportion of swellable clays and a low proportion of non-swellable clays. Weimann (2001) attributed the disjoining pressure as a main cause for moisture expansion evident in rocks such as granite and marble, which are clay-poor or free of swellable clay minerals (Schult and Shi 1996; Weiss 1992). Ruedrich et al. (2011) suggested the possibility of disjoining pressure in rocks, especially under the presence of micropores with sizes of 0.1 µm. The disjoining pressure evolves from a combination of processes that cause the repulsion of the two interfaces. The source of the pressure can be electrostatic interactions, for example, dispersion forces, hydration forces and the overlap of electrical double layers (Butt et al. 2003; Jamtveit & Hammer 2012). For cement stones that are negatively charged, water molecules attach themselves to pore gusset and elongated pores, which are thus under pressure. This disjoining pressure causes swelling deformation. Pötzl et al. (2018a) showed this swelling deformation for the Hilbersdorf tuff variety (HR), which has the strongest hydric strain with 2.24 mm/m, but no swelling clay minerals. Clay mineral associated swelling was consequently excluded. When analyzing the pore radius distribution, it is noticeable that the variety HR has pores in the range < 2 nm. Sandstones, like the Sander contains traces of expandable illite-rich, illite–smectite mixed layers together with chlorite, illite, and kaolinite. Schleerieth contains chlorite and illite.

There is no correlation between the average pore radius and the extent of moisture expansion as can be seen in Fig. 26A. Regarding the average values for the hygric expansion a weak correlation with the micropores can be observed. The sandstone Villarlod and the tuff Cantera Verde do not fit the slight observable tendency, that the higher the microporosity, the larger is the moisture swelling magnitude (Fig. 26B). Thus, the main cause of the swelling and shrinking due to changes in moisture content can be the disjoining pressure in small pores. This may be true for the Sander and Schleerieth sandstones. These rocks have a microporosity of 41% and 47%. Especially for the Schleerieth this process should be important because there are no swellable clay minerals. Only in the large percentage of lithoclasts (approx. 15%) could such minerals occur. Sorption can be used to characterize the hygroscopic water absorption of sandstones. In the course of the weight increase (sorption) between 15% and approximately 80% rel. humidity, the Schleerieth and Sander show a linear increase, from 80% to approximately 95%, which is a clear steepening of the curves. A high proportion of micropores in the total porosity is decisive for the degree of saturation or sorption at high humidity (Fig. 25). Even at high air humidity, capillary condensation and the associated full saturation of the pores only takes place in micropores. In larger pores, only the formation of a multimolecular water film on the pore walls occurs (Weimann 2001). Sorption occurs almost exclusively in the small pores (< 0.001 m) at low humidity and results in elongation of the saturated pores. These two sandstones show long-lasting elongation despite a moderate *w*-value and water vapor resistance, respectively. The tuffs such as the BP, LOS, BS and the CV have a pronounced microporosity (90%) of up to 13.41% by volume (see Fig. 25), as in the case of the Blue Sevan. However, these tuffs have swellable clay minerals such as smectites and illite–smectite-mixed layers. Therefore, intracrystalline swelling is of particular importance for these tuffs, although disjoining pressure cannot be excluded, but could occur as a secondary mechanism.

The Noyemberyan tuff also does not have too much illite–smectite mixed layers but many zeolites. The microporosity is 9.5 vol%. Fluid exchange with salt solutions shows that osmotic swelling is not important. A small amount of disjoining pressure cannot be ruled out, however, intracrystalline swelling is the controlling mechanism.

From our investigations it becomes clear that the quantification of the hygric strain with respect to its mode, i.e. the controlling process, is quite complex, but can be elucidated. However, a quantification of the individual proportions of intracrystalline and osmotic swelling as well as the disjoining pressure seems to be not possible from our observations, i.e. a qualitative estimation is the best approach at the moment.

By selectively replacing the interlayer cations in the clay minerals and subsequently changing the swelling behavior of the rocks, it was demonstrated that the intracrystalline swelling mechanism is the predominant mechanism for swelling in the investigated tuffs and sandstones with swellable clay minerals. Confirmation of the intracrystalline swelling process is achieved by selectively blocking the hydration of the clay mineral interlayers and thereby suppressing their expansion (Figs. 12, 13, 14). A second swelling test, in which fluid exchange served to verify intercrystalline or osmotic swelling, confirmed the almost insignificant contribution of osmotic swelling to the overall swelling process. In all

the rocks studied, with the exception of the zeolite-bearing variants, the proportion of osmotic swelling is of minor importance.

Disjoining pressure is discussed and documented for the rocks types without swellable clay minerals. The reason for the very different swelling behavior of the rocks is the mineralogical composition of the samples, their heterogeneity in regard to volcanic tuffs and the varying rock fabrics. A striking feature is the different modes of occurrence for zeolites in the rocks (Table 3; Figs. 18I, 19A, B, D, E). The treatment with sodium chloride causes a reduced expansion in all investigated samples compared to the untreated samples. This behavior is also opposite to the enhanced swelling behavior described in Wangler and Scherer (2008) and Pötzl et al. (2018a).

Concluding statements

The physical process of swelling and shrinkage caused by frequent wetting and drying cycles is often considered a very significant cause of damage to the weathering of clay-bearing sandstones and volcanic tuffs. Based on the observations and experimental results in this study, a number of concluding statements can be made concerning the hydric expansion in volcanic tuffs and sandstones.

1. Both volcanic tuffs and sandstones show diverse heterogeneous and anisotropic rock fabrics and contain varied mineralogical compositions. In volcanic tuffs, these differences in rock fabrics are the direct result of the volcanic eruption and the deposition of the erupted material both near and far from the volcanic event. These pyroclastic rocks, such as those in this study from Armenia and Mexico contain pumice fragments, lapilli, relict glass shards, an ash-rich or cryptocrystalline groundmass, and in some cases a sedimentary layering (e.g., the volcanoclastic Loseros tuff), all of which contribute to the diverse heterogenous rock fabrics. The weathering of these rocks leads to the development of clay minerals and zeolites by the alteration of vitric components or the alteration of pumice fragments to clay (e.g., the volcanic clasts in Noyemberyan).

   Sandstones are also formed in many different depositional environments, which leads to various grain sizes, types of grading, the sorting of grains and the development of sedimentary layering. They show diverse mineralogical compositions depending upon their depositional environment of formation. Examples include the fossil-rich calcareous Baumberger sandstone, the glauconite-bearing Villarlod molasse sandstone or the Schleerieth sandstone containing a higher percentage of lithoclasts. The weathering of lithoclasts may be a source for the formation of swellable clay minerals.
2. In the literature, clay minerals in particular are held responsible for explaining the hygric expansion processes, especially in volcanic tuffs and sandstones. Here it should first be pointed out that there are swellable and non-swellable clay minerals. Swellable clay minerals contain large reactive surface areas and these interlayer regions are called smectitic interlayers. Their swelling potential is by far, higher than that of minerals with non-smectitic surfaces such as kaolinite, chlorite, illite, and vermiculite. Layers of individual units of these listed clay minerals can be stacked on each other in variable amounts and with variable degrees of ordering; these minerals are called interstratified or mixed layers, however, for swelling potential only the amount of reactive smectitic surfaces is responsible for the inner-crystalline swelling largely exceeding osmotic swelling. The CEC is a very good measure for the amounts of smectitic layers as the CEC of smectite is much larger than of all the other clay minerals typical for tuffs and sandstones.
3. The zeolite-group of minerals are of special importance in volcanic rocks but also for sandstones, if volcanic lithoclasts are part of the compositional makeup. Natural zeolites are minerals of magmatic origin or the result of, for example, metamorphic and/or hydrothermal overprinting. Due to their crystal structure they can show a higher cation exchange capacity, i.e., zeolites have the ability to exchange and bind cations at negatively charged places on the surface. On the other hand, the CEC of zeolites is very low when determined with large complexes such as Cu-trien used in this study, whereas other index cations may give CEC values larger than smectites. The swelling pressure developed by cation exchange and hydration of interlayer cations cannot be compared with that of swellable clay minerals because most of the cations will be exchanged in the inner surfaces of zeolites. Volume changes of these tectosilicates are much smaller compared to the volume changes by the swelling of phyllosilicates.
4. The type and location of clay minerals play a significant role as a damage-causing factor in tuffs and sandstones by the mechanism of intracrystalline swelling. Clay minerals such smectite, poorly ordered smectitic mixed-layer and well-ordered smectite-rich corrensite are the swellable clay minerals responsible for the damages in the investigated rocks. When swellable clay minerals are located at grain contacts, filling or coating micropores, coat mineral grains or are aligned parallel to the grain boundaries in layered fine-grained ash-rich tuffs or sandstones, moisture-induced expansion

occurs, leading to stresses in the rock fabric. This leads to the various types of damages observed in the investigated rocks. However, when swellable clay minerals are located in macropores, such as those found in volcanic tuffs, the swelling clay will have enough space to freely expand, and thus no damage may occur. Moreover, when no swellable clay minerals are present, such as in the Schleerieth sandstone, another mechanism is responsible for the damage to the rock fabric. This study proposes that disjoining pressure (or cleavage pressure) leads to the measured hydric expansion in the Schleerieth sandstone.

5. From our overview of the literature, the two terms, hygric- and hydric expansion are mostly interchangeably used to define moisture expansion. We have observed that the term hygric expansion is mainly used to describe the phenomena of moisture expansion, while hydric expansion is less common. To summarize, in most cases when measuring the moisture expansion the samples are immersed in a water tray with a specific water level. The moisture expansion as a function of relative humidity from 0 to 95% is seldom reported. To avoid further confusion in the future, we would suggest that the term hydric expansion should refer to the moisture expansion or swelling behavior, and in general, when the effect of RH is discussed, the term hygric expansion should be subscripted or placed in brackets.
6. When clay minerals or zeolites are present in a building stone, two swelling mechanisms are under discussion: (1) intracrystalline, or simply crystalline; and (2) inter-crystalline, inter-particle or osmotic swelling. The moisture expansion mode can be experimentally investigated by the pre-treatment of the samples with various cations. Sodium, calcium, magnesium, cesium, etc. can have different effects on the swelling behavior and point to the intracrystalline swelling process. Osmotic swelling processes can be detected when the water of fully swollen stone samples were syringed out and replaced with a salt solution. When rocks without any swellable minerals show any moisture expansion a disjoining pressure as a controlling process is discussed.
7. Various stone properties can be used as indications for the swelling and drying behavior. The porosity and especially the pore radius distribution are important. A high proportion of micropores can be used to assess disjoining pressure. With a very high proportion of capillary pores and a correspondingly high capillary water absorption behavior, this hygric mode will be insignificant.
8. Hygric expansion and the total water absorption are critical parameters for damage to natural stone. Hygric expansion occurs not only when directly wetted with water but also when the relative humidity changes. In this case, a high amount of expansion can also be observed. These are generally lower, however, as compared to those that occur through direct wetting with water. The intensity of the hygric expansion in the partially saturated moisture range varies greatly depending on the material. In laboratory tests on hygric expansion, a very strongly varying time dependence of the expansion can be determined for different materials. This is essentially due to the varying pore space properties of the respective rocks. Rocks with well cross-linked pores and relatively high porosity show a fast expansion, whereas less well cross-linked rocks swell more slowly.
9. The permanent moisture load and the associated pollutant input can lead to the formation of scaling and flaking phenomena parallel to the surface. Further examples that lead to this phenomenon include salt crystallization or the dissolution or transformation of rock-internal minerals like Fe-hydroxide formation, transport and precipitation. Scaling formation or flaking parallel to the sedimentary bedding or to any flow fabrics in volcanic rocks can show preferential damage patterns by the swelling strain. The dynamic Young's modulus for the investigated rocks varies between approximately 10 and 33 GPa. The strength properties, especially the tensile strengths, range between approximately 1.9 MPa and 7.0 MPa under dry conditions. Under water-saturated conditions, there is an additional drastic reduction in strength of approximately a factor of 2–3. For an average hygric expansion of 0.5 mm/m, an expansion pressure of 10 MPa is calculated on the basis of a Young's modulus of 20 GPa. This expansion pressure is already higher than the tensile strength of the examined rock in the dry state. With a hygric expansion of 1 mm/m and more and significantly lower elastic moduli or tensile strengths, the typical damage pattern due to hygric expansion are definitely to be expected.
10. The knowledge of hygric expansion processes and their damage-controlling properties is particularly important when historically valuable natural stone objects made of sandstones and volcanic tuffs should be conserved. For this purpose, it is absolutely necessary to know the absolute magnitude of the swelling strain, even with the addition of so-called anti-swelling agents and the corresponding consolidation products. In addition, such processes are of particular importance if zeolites are also present in addition to the usually known phyllosilicate clay minerals. The principles of action of the different consolidation treatments to be applied are particularly critical for the extremely heterogene-

ous group of tuffs, as the range of possible property changes with regard to hygric expansion and the consolidation to be added must be known.

Acknowledgements We are grateful to Christopher Pötzl and Johanna Menningen for the laboratory support and help with the analyses of the physical properties. Furthermore, we would like to thank G. Buntebarth for the preparation and production of the model samples used in the swelling experiments. We thank R. Lopez-Doncel for the help with the sampling and sample transfer to Germany. We are very grateful to Mathilde Tiennot and Danielle-Marjorie Ducotterd for the photo showing the decay phenomena on the City Hall of Fribourg (Switzerland) and Ulrich Kaplan (Gütersloh) for the Baumberger decay photo. This work was supported by the German Research Foundation (Si-438/52-1) and the Volkswagen Foundation (AZ:93919).

Author contributions All authors had significantly contributed to the manusscript

Funding Open Access funding enabled and organized by Projekt DEAL. The authors have not disclosed any funding.

Availability of data and materials All data are available on request from the authors.

Declarations

Competing interests The authors declare no competing interests.

References

Bache BW (1965) The thermodynamics of soil phosphate. Oil phosphorus. Min Agric Technol Bull 13:10–18

Bailey SW (1980) Summary of recommendations of AIPEA Nomenclature Committee on clay minerals. Am Mineral 65:1–7

Barrer RM (1978) Zeolites and clay minerals as sorbents and molecular sieves. Academic Press, London

Barrer RM, Klinowski K (1972) Ion exchange involving several groups of homogeneous sites. J Chem Soc Faraday Trans I 68:73–87

Beaufort D, Baronnet A, Lanson B, Meunier A (1997) Corrensite: a single phase or a mixed-layer phyllosilicate in the saponite-to-chlorite conversion series? A case study of Sancerre-Couy deep drill hole (France). Am Mineral 82:109

Benavente D, Cultrone G, Gómez-Heras M (2008) The combined influence of mineralogical, hygric and thermal properties on the durability of porous building stones. Eur J Mineral 20(4):673–685

Bergaya F, Lagaly G, Vayer M (2006) Chapter 12.10 cation and anion exchange. In: Bergaya F, Theng BKG, Lagaly G (eds) Developments in clay science. Elsevier, New York, pp 979–1001

Blöchl B, Kirchner D, Stadlbauer E (1998) Die hygrische Dehnung von Baumberger Kalksandsteinen-tonmineralogische und gesteinsphysikalische Aspekte. Arbeitshefte Zur Denkmalpflege in Niedersachsen 15:46–55

Bock H, Dehandschutter B, Martin CD, Mazurek M, de Haller A, Skoczylas F, Davy C (2010) Self-sealing of fractures in argillaceous formations in the context of geological disposal of radioactive waste. NEA 6184. Nuclear Energy Agency Organization for Economic Co-Operation and Development

Bosbach D, Hochella MF Jr (1996) Gypsum growth in the presence of growth inhibitors: a scanning force microscopy study. Chem Geol 132(1–4):227–236

Bosbach D, Junta-Rosso JL, Becker U, Hochella MF Jr (1996) Gypsum growth in the presence of background electrolytes studied by scanning force microscopy. Geochim Et Cosmochim Acta 60(17):3295–3304

Butt H, Graf K, Kappl M (2003) Physics and chemistry of interfaces, chapter surface forces. WILEY-VCH GmbH and Co. KGaA, New York, pp 80–116

Cavazos-Álvarez JA, Carrasco-Núnez G, Dávila-Harris P, Pena D, Jáquez A, Arteaga D (2020) Facies variation and permeability of ignimbrites in active geothermal systems; case study of the Xáltipan ignimbrite at Los Humeros Volcanic Complex. J S Am Earth Sci 104:102810

De la Calle C, Suquet H (1988) Vermiculite. Rev Mineral Geochem 19:455–496

Demarco MM, Jahns E, Ruedrich J, Oyhantçabal P, Siegesmund S (2007) The impact of partial water saturation on rock strength: an experimental study on sandstone. Z Dt Ges Geowiss 158(4):869–882

Derjaguin BV, Kusakov MM (1936) The properties of thin layers of liquids. Proc Acad Sci USSR Chem Ser 5:741–753

DIN 66133 (1993) Bestimmung der Porenvolumenverteilung und der spezifischen Oberfläche von Feststoffen durch Quecksilberintrusion. Beuth, Berlin

DIN EN 772-4 (1998) Prüfverfahren für Mauersteine-Teil 4: Bestimmung der Dichte und der Rohdichte sowie der Gesamtporosität und der offenen Porosität von Mauersteinen aus Naturstein. Beuth, Berlin

DIN 13009 (2000) Bestimmung des hygrischen Dehnkoeffizienten. Beuth, Berlin

DIN EN ISO 12572 (2017) Bestimmung der Wasserdampfdurchlässigkeit. Beuth, Berlin

Dixon JB, Weed SB (1989) Minerals in soil environments, 2nd edn. Soil Science Society of America, Madison

Doebelin N, Kleeberg R (2015) Profex: a graphical user interface for the Rietveld refinement program BGMN. J Appl Crystal 48:1573–1580

Dohrmann R, Kaufhold S (2009) Three new, quick CEC methods for determining the amounts of exchangeable calcium cations in calcareous clays. Clays Clay Miner 57:338–352

Dohrmann R, Kaufhold S (2010) Determination of exchangeable calcium of calcareous and gypsiferous bentonites. Clays Clay Miner 58:79–88

Dohrmann R, Genske D, Karnland O, Kaufhold S, Kiviranta L, Olsson S, Valter M (2012) Interlaboratory CEC and exchangeable cation study of bentonite buffer materials: I. Cu(II)-triethylenetetramine method. Clays Clay Miner 60:62–175

Elert K, Rodriguez-Navarro C (2022) Degradation and conservation of clay-containing stone: a review. Constr Build Mater 330:127226

Farrell NJC, Healy D (2017) Anisotropic pore fabrics in faulted porous sandstones. J Struc Geol 104:125–141
Filippidis A, Kantiranis N, Stamatakis M, Drakoulis A, Tzamos E (2007) The cation exchange capacity of the Greek zeolitic rocks. Bull Geol Soc Greece 40:723–735 (Proceedings of the 11th International Congress, Athens, Greece, 2007)
Fisher RV (1966) Rocks composed of volcanic fragments and their classification. Earth Sci Rev 1:287–298
Fitzner B (1988) Untersuchung der Zusammenhänge zwischen dem Hohlraumgefüge von Natursteinen und physikalischen Verwitterungsvorgängen. Mitt Ing -u Hydrogeologie, 29, Aachen
Fitzner B, Snethlage R (1982) Einfluss der porenradienverteilung auf das verwitter ungsverhalten ausgewählter Sandsteine. Bautenschutz+ Bausanierung, pp 97–103
Graf v Reichenbach H, Beyer J (1995) Dehydration and rehydration of vermiculites. II: Phlogopitic Ca-vermiculite. Clay Min 30:273–286
Grassegger, G (1998) Mineralogische Prozesse bei der Bausteinverwitterung. In: Denkmalpflege und Naturwissenschaft, Natursteinkonserverung II. Fraunhofer IRB Verlag, Stuttgart, pp 119–137
Grimm W (1968) Eine neue Glimmentladungslampe für die optische Emissionsspektralanalyse. Spectrochimica Acta Part B: Atomic Spectroscopy 23(7):443–454
Grimm WD (2018) Bildatlas wichtiger Denkmalgesteine der Bundesrepublik Deutschland/Wolf-Dieter Grimm; Teil I & Teil 2. Ebner Verlag Ulm. 1-440, 1-536
Guggenheim S, Adams JM, Bain DC, Bergaya F, Brigatti MF, Drits VA, Formoso MLL, Galán E, Kogure T, Stanjek H (2006) Summary of recommendations of Nomenclature Committees relevant to clay mineralogy: report of the association Internationale pour l'Etude des Argiles (AIPEA) Nomenclature Committee for 2006. Clays Clay Miner 54:761–772
Hirschwald J (1912) Die Prüfung der natürlichen Bausteine auf ihre Wetterbeständigkeit. W. Ernst und Sohn, Berlin
Jamtveit B, Hammer O (2012) Geochemical perspectives. European Association of Geochemistry
Kahr G, Kraehenbuehl F, Müller-Vonmoos M, Stoeckli HF (1986) Wasseraufnahme und Wasserbewegung in hochverdichtetem Bentonit (No. 86-14). ETH Zurich
Kaufhold S, Baille W, Schanz T, Dohrmann R (2015) About differences of swelling pressure—dry density relations of compacted bentonites. Appl Clay Sci 107:52–61
Kettelhack C (1992) Mikrofazies des Altenberger Steins und des Baumberger Sandsteins sowie ihre Verwitterungserscheinungen dokumentiert an zwei historischen Baudenkmälern in Münster/Westf. Dissertation, University of Münster
Kleeberg R, Monecke T, Hillier S (2008) Preferred orientation of mineral grains in sample mounts for quantitative XRD measurements: how random are powder samples? Clays Clay Miner 56:404–415
Kocher M (2005) Quelldruckmessungen und thermische Druckmessungen an ausgewählten Sandsteinen. Dissertation, University of München
Koyama K, Takeuchi Y (1977) Clinoptilolite: the distribution of potassium atoms and its role in thermal stability. Z Kristallogr Cryst Mater 145(1–6):216–239
Kraus K (1985) Experimente zur immissionsbedingten Verwitterung der Naturbausteine des Kölner Doms im Vergleich zu deren Verhalten am Bauwerk. Dissertation, University of Cologne
Le Bas MJ, Le Maitre RW, Streckeisen A, Zanettin B (1986) A chemical classification of volcanic rocks based on the total alkali-silica diagram. J Petrol 27:745–750
López-Doncel R, Wedekind W, Dohrmann R, Siegesmund S (2013) Moisture expansion associated to secondary porosity: an example of the Loseros Tuff of Guanajuato, Mexico. Environ Earth Sci 69:1189–1201
McBride EF (1963) A classification of common sandstones. J Sed Petrol 33(3):664–669
Meier LP, Kahr G (1999) Determination of the cation exchange capacity (CEC) of clay minerals using the complexes of copper(II) ion with triethylenetetramine and tetraethylene petamine. Clays Clay Miner 47:386–388
Mitchell JK (1993) Fundamentals of soil behavior, 2nd edn. Wiley, Hoboken
Monecke T, Köhler S, Kleeberg R, Herzig PM, Gemmell JB (2001) Quantitative phase-analysis by the Rietveld method using X-ray powder-diffraction data: application to the study of alteration halos associated with volcanic-rock-hosted massive sulfide deposits. Can Miner 39:1617–1633
Moore DM, Reynolds RC Jr (1989) X-ray diffraction and the identification and analysis of clay minerals. Oxford University Press, Oxford
Nägele E, Kraus K, Legrum J (1992) Die Rolle von Salzen bei der Verwitterung von mineralischen Baustoffen. WTA-Schriftenreihe, Heft
Pahlke H (2012) Die Dynamik von Wasser in Zeolithen. Dissertation, Technische Universität Darmstadt
Pina CM, Bosbach D, Prieto M, Putnis A (1998) Microtopography of the barite (0 0 1) face during growth; AFM observations and PBC theory. J Cryst Growth 187(1):119–125
Pötzl C, Dohrmann R, Siegesmund S (2018a) Clay swelling mechanism in tuff stones: an example of the Hilbersdorf Tuff from Chemnitz, Germany. Environ Earth Sci 77:188
Pötzl C, Siegesmund S, Dohrmann R, Koning JM, Wedekind W (2018b) Deterioration of volcanic tuff rocks from Armenia: constraints on salt crystallization and hydric expansion. Environ Earth Sci 77:660
Pötzl C, Rucker S, Wendler E, Siegesmund S (2022a) Consolidation of volcanic tuffs with TEOS and TMOS: a systematic study. Environ Earth Sci 81:1–27
Pötzl C, Siegesmund S, López-Doncel R, Dohrmann R (2022b) Key parameters of volcanic tuffs used as building stone: a statistical approach. Environ Earth Sci 81:1–29
Pusch R, Börgesson L, Frederiksson A, Johannesson LE, Hökmark H, Karnland O, Sandén T (1995) The buffer and backfill handbook. Tech Rept 95-45, SKB, Clay Technology AB
Putnis A, Maute G (2000) The effect of pore size on cementation in porous rocks. Geofluids 1:37–41
Putnis A, Prieto M, Fernandez-Diaz L (1995) Supersaturation and crystallisation in porous media. Geol Mag 132:1–13
Rietveld HM (1969) A profile refinement method for nuclear and magnetic structures. J Appl Crystallogr 2:65–71
Rodriguez-Navarro C, Doehne E (1999) Salt weathering: influence of evaporation rate, supersaturation and crystallization pattern. Earth Surf Process Landf J Br Geomorphol Res Group 24(3):191–209
Rousset B, Bläuer C (2009) R. 0014.01 f: Cathédrales de bâle, de Berne, de Fribourg et de Lausanne: project de contrôle et de suivi des consolidants: résultats des teste de laboratoire. Tech Rep Conserv Sci Consult Sàrl
Ruedrich J, Siegesmund S (2006) Fabric dependence of length change behaviour induced by ice crystallisation in the pore space of natural building stones. Proceedings international conference, heritage, weathering and conservation. pp 497–505
Ruedrich J, Bartelson T, Dohrmann R, Siegesmund S (2011) Moisture expansion as a deterioration factor for sandstone used in buildings. Environ Earth Sci 63:1545–1564
Schmid R (1981) Descriptive nomenclature and classification of pyroclastic deposits and fragments: recommendation of the IUGS Sub-commission on the systematics of igneous rocks. Geol 9:41–43
Schult A, Shi G (1996) Hydration swelling of crystalline rocks. Geophys J Int 131(1):179–186

Sebastián E, Cultrone G, Benavente D, Fernandez LL, Elert K, Rodriguez-Navarro C (2008) Swelling damage in clay-rich sandstones used in the church of San Mateo in Tarifa (Spain). J Cult Herit 9(1):66–76

Siedel H (1994) Untersuchungen und Restaurierungskonzeption zur Tulpenkanzel im Dom zu Freiberg (Sachsen) unter besonderer Berücksichtigung der Entsalzung. Arbeitsblätter für Restauratoren, Mainz 2, Gruppe 6, Stein. pp 307–312

Siedel H (1998) Zur Verwitterung des Rochlitzer Porphyrtuffs an der Kunigundenkirche in Rochlitz. Jahresberichte Steinzerfall-Steinkonservierung für 1994–1996. IRB Verlag, Stuttgart, pp 335–344

Siedel H (2010) Historic building stones and flooding: changes of physical properties due to water saturation. J Perform Constr Facil 24(5):452–461

Siegesmund S, Dürrast H (2014) Physical and mechanical properties of rocks. In: Siegesmund S, Snethlage R (eds) Stone in architecture: properties, durability, 5th edn. Springer, Berlin, pp 97–224

Siegesmund S, Snethlage R (eds) (2014) Stone in architecture: properties, durability. Springer Science & Business Media, Berlin

Siegesmund S, Grimm WD, Dürrast H, Ruedrich J (2010) Limestones in Germany used as building stones: an overview. Geol Soc Lond Spec Pub 331:37–59

Snethlage R, Wendler E (1997) Moisture cycles and sandstone degradation. Environ Sci Res Rep ES 20:7–24

Snethlage R, Wendler E, Klemm DD (1995) Tenside im Gesteinsschutz-bisherige Resultate mit einem neuen Konzept zur Erhaltung von Denkmälern aus Naturstein. Denkmalpflege und Naturwissenschaft-Natursteinkonservierung I. Verlag Ernst & Sohn, Berlin, pp 127–146

Sridharan A, Rao S, Sivapullaiah PV (1986) Swelling pressure of clays. ASTM Geotech Test J 9:24–33

Steiger M, Charola AE, Sterflinger K (2011) Weathering and deterioration. In: Siegesmund S, Snethlage R (eds) Stone in architecture. Springer, Berlin, pp 227–316

Stockhausen N (1981) Die Dilatation hochporöser Festkörper bei Wasseraufnahme und Eisbildung. Dissertation, TU München

Stück H, Koch R, Siegesmund S (2013) Petrographical and petrophysical properties of sandstones: statistical analysis as an approach to predict material behaviour and construction suitability. Environ Earth Sci 69:1299–1332

Tiennot M, Bourgès A, Mertz JD (2016) Influence of the Villarlod Molasse Anisotropy on cracking advances in the comprehension of the desquamation mechanisms. Sci Art A Future Stone 155

Tiennot M, Mertz JD, Bourgès R (2019) Influence of clay minerals nature on the hydromechanical and fracture behaviour of stones. Rock Mech Rock Eng 52:1599–1611

Ufer K, Kleeberg R, Bergmann J, Dohrmann R (2012a) Rietveld refinement of disordered illite-smectite mixed-layer structures by a recursive algorithm. I: one-dimensional patterns. Clays Clay Miner 60:507–534

Ufer K, Kleeberg R, Bergmann J, Dohrmann R (2012b) Rietveld refinement of disordered illite-smectite mixed-layer structures by a recursive algorithm. II: powder-pattern refinement and quantitative phase analysis. Clays Clay Miner 60:535–552

van Bemmelen JM (1888) Über die Adsorptionsverbindungen und das Absorptionsvermögen der Ackererde. Landwirtsch Versuchsstation 35:69–136

Visser H, Mirwald P (1998) Baumberger Kalksandstein-Materialeigenschaften und Schadenspotential. Arbeitshefte Zur Denkmalpflege Niedersachsen 15:28–45

Wangler T (2016) Swelling clay and its inhibition in the Villarlod molasse. Sci Art A Future for Stone 189

Wangler T (2020) Mechanism of clay swelling in Villarlod molasse, a Swiss sandstone. https://doi.org/10.31224/osf.io/s3d46

Wangler T, Aguilar Sanchez AM (2020) Potential damage mechanism in Swiss molasse. In. Siegesmund S, Middendorf R (eds) Monument future: decay and conservation of stone. Proceedings of the 14th international congress on the deterioration and conservation of stone. Mitteldeutscher Verlag, pp 501–506

Wangler T, Scherer GW (2008) Clay swelling mechanism in clay-bearing sandstones. Environ Geol 56:529–534

Weimann MB (2001) Hygrische Eigenschaften von Polymerbeton im Vergleich mit porösen mineralischen Werkstoffen des Bauwesens. Dissertation, ETH Zurich

Weiss A (1958) Der Kationenaustausch bei den Mineralen der Glimmer-, Vermiculit- und Montmorillonitgruppe. Z Anorg Allgem Chem 297:257–360

Weiss G (1992) Die Eis und Salzkristallisation im Porenraum von Sandsteinen und ihre Auswirkung auf das Gefüge unter besonderer Berücksichtigung gesteinsspezifischer Parameter. Münchner Geowissenschaftliche Abhandlungen, Reihe B, 9: 62

Weiss T, Siegesmund S, Kirchner DT, Sippel J (2004) Insolation weathering and hygric dilatation: two competitive factors in stone degradation. Environ Geol 46(3):402–413

Wendler E (1991) Zum Mechanismus der Schalenbildung bei tonigen Sandsteinen. Jahresberichte Steinzerfall-Steinkonservierung für 1989. Verlag Ernst & Sohn, Berlin, pp 71–76